

Pareto sensitivity, most-changing sub-fronts, and knee solutions

T. Giovannelli*

M. M. Raimundo[†]L. N. Vicente[‡]

March 23, 2026

Abstract

When dealing with a multi-objective optimization problem, obtaining a comprehensive representation of the set of Pareto optimal solutions can be computationally expensive. However, identifying the most representative solutions can be difficult and sometimes ambiguous, since what constitutes a representative solution depends on the decision maker's preferences. A popular selection are the so-called Pareto knee solutions, which correspond to nondominated points on the Pareto front where a small improvement in any objective leads to a large deterioration in at least one other objective. In this paper, using Pareto sensitivity, we show how to compute Pareto knee solutions according to their verbal (informal) definition of least maximal change. We refer to the resulting approach as the *sensitivity knee* (snee) approach, and we apply it to unconstrained and constrained problems. Pareto sensitivity can also be used to compute local most-changing Pareto sub-fronts around a nondominated point, where points on the sub-fronts are distributed along directions of maximum change. Our approach is still restricted to scalarized methods, in particular to the weighted-sum or epsilon-constrained methods, and requires the computation or approximations of first- and second-order derivatives. We include numerical results from synthetic problems that illustrate the benefits of our approach.

1 Introduction

In this paper, we focus on the following multi-objective optimization (MOO) problem

$$\min_{x \in X \subseteq \mathbb{R}^n} F(x) = (f_1(x), \dots, f_q(x)), \quad (1.1)$$

where each $f_i : \mathbb{R}^n \rightarrow \mathbb{R}$ is a twice continuously differentiable function for all $i \in \{1, \dots, q\}$, with $q \geq 2$, and X represents the feasible set, which is either $X = \mathbb{R}^n$ in the unconstrained case or a subset $X \subset \mathbb{R}^n$ in the constrained case. Problems with multiple objectives find applications across a wide range of domains. In engineering design, multiple objectives correspond to various performance measures (e.g., efficiency, reliability, and safety) that must be maximized simultaneously [14, 29, 37, 39, 65]. In finance, MOO is at the heart of portfolio optimization problems, where the trade-offs between risk and return need to be balanced to achieve the best investment strategy [13, 64, 66]. In the healthcare sector, MOO is used

*Department of Mechanical, Materials, and Industrial Engineering, University of Cincinnati, Cincinnati, OH 45221, USA (giovanto@ucmail.uc.edu).

[†]Departamento de Sistemas de Informação, UNICAMP - Universidade Estadual de Campinas, Campinas, São Paulo, Brasil (mraimundo@ic.unicamp.br).

[‡]Department of Industrial and Systems Engineering, Lehigh University, Bethlehem, PA 18015-1582, USA (lnv@lehigh.edu).

to strike a balance between providing equitable or rapid service to patients and managing operational costs effectively [7, 73]. In transportation systems, MOO helps optimize routing and speed decisions to minimize environmental impact while maximizing efficiency for service providers and ensuring high service quality for users [25, 32]. In the field of machine learning, MOO problems are particularly relevant in scenarios like multi-task learning [11, 46], where a model must perform well on several related conflicting tasks simultaneously, and in learning problems that address fairness and privacy concerns [49, 51].

We now introduce terminology that will be used throughout Subsections 1.1 and 1.2, and formally defined in Definitions 1 and 2 of Section 2. Specifically, the optimal solutions to problem (1.1) are referred to as Pareto optimal solutions or efficient solutions, and the set of all such solutions is called the efficient set. The Pareto front of problem (1.1), also referred to as the nondominated set or Pareto set, is the set obtained by mapping the Pareto optimal solutions from the decision space \mathbb{R}^n to the objective space \mathbb{R}^q . Each point on the Pareto front is referred to as a nondominated point.

1.1 Finding relevant Pareto optimal solutions

Determining a large number of Pareto optimal solutions can be computationally expensive and redundant, particularly with a high number of objectives [47, 70]. While all Pareto optimal solutions are mathematically valid solutions, it is generally preferable to identify only a few representative solutions [6, 68]. Well-known multi-criteria decision-making techniques have been proposed for selecting a single Pareto optimal solution. *A priori methods* [26, 50] consist of reducing an MOO problem into a single-objective one by incorporating user preferences, which can be achieved by either weighting the objective functions into a single function with user-defined weights (weighted-sum method), minimizing one objective function and considering the other objectives as constraints with user-defined right-hand sides (ϵ -constraint method), minimizing a user-defined utility function (utility-based method), or minimizing the deviation of the objectives from user-defined target values (also known as goal programming). The so-called *knee solutions*¹ [10, 18, 21, 50] are Pareto optimal solutions that correspond to nondominated points on the Pareto front where a small improvement in any objective would lead to a large deterioration in at least one other objective, which is a commonly-used **verbal (informal) definition**. *Sharpe solutions* [48, 61] have only been proposed for bi-objective problems and are defined as Pareto optimal solutions with the smallest function value in the first objective per unit of function value in the second objective.

In addition to a priori methods, other widely studied classes of multi-criteria decision-making approaches include *a posteriori* and *interactive methods* [1, 26, 50]. A posteriori methods aim to approximate the entire set of Pareto optimal solutions (i.e., the efficient set), after which a decision maker selects a preferred solution in a post-processing step. Interactive methods iteratively generate Pareto optimal solutions while progressively incorporating decision-maker preferences throughout the optimization process. However, the primary goal of these approaches is not the direct identification of a single representative Pareto optimal solution, but rather the approximation of the entire efficient set.

In this work, we focus on knee solutions, which we identify using a sensitivity-based approach that does not require explicit user preferences (unlike a priori methods), applies to an arbitrary number of objective functions (unlike Sharpe solutions), avoids computing an approximation of the efficient set (unlike a posteriori methods), and does not involve iterative interaction with a decision maker (unlike interactive methods). Knee solutions have gained significant popularity and have been extensively studied in the literature. A review of methods to compute knee solutions (and the corresponding knee

¹Throughout this paper, we interpret a (*Pareto*) *knee solution* as a Pareto optimal solution in the decision space \mathbb{R}^n , and refer to the corresponding nondominated point in the objective space \mathbb{R}^q as a *knee nondominated point*.

nondominated points) is provided in [9] and [22]. However, a widely accepted (quantitative) definition for such solutions is lacking, and identifying knee solutions in high-dimensional objective spaces remains challenging. Furthermore, as discussed in Deb and Gupta [22, Subsection 2.2], most current methods identify nondominated points that do not necessarily correspond to knee solutions based on the verbal definition, but are simply intermediate points on the Pareto front, where the trade-off between the improvement in any objective and the corresponding deterioration in at least one other objective is not necessarily significant. Throughout this paper, following terminology adopted in [22], we refer to the intermediate region of the Pareto front as the set of nondominated points that do not lie on its boundary. These concepts will be defined more formally in Section 2.

Existing methods for determining knee solutions generally fall into three categories: angle-based, utility-based, and normal boundary intersection-based approaches. Such methods are described below, highlighting their motivations and limitations. Our sensitivity-based approach, which is alternative to these three categories, is described in Subsection 1.2.

Angle-based methods, which are applicable only to problems with two objective functions, identify knee nondominated points by measuring reflex angles [9] or bend angles [22] using a predetermined set of nondominated points. Specifically, a reflex angle is formed between a nondominated point and two chosen neighboring nondominated points (one to the left and one to the right). Since a reflex angle is determined using neighboring solutions, it reflects a local characteristic of the Pareto front, describing its behavior in the vicinity of a specific nondominated point. A bend angle is similar to a reflex angle but is obtained by replacing neighboring nondominated points with extreme points of the Pareto front², which are nondominated points that correspond to the minimizers of each objective function individually. Since a bend angle is calculated using extreme nondominated points of the Pareto front, it is better able to capture the global behavior of the Pareto front. In general, reflex and bend angles approximate the shape of the Pareto front at a given nondominated point, and the knee solution is the Pareto optimal solution corresponding to the nondominated point with the maximum reflex or bend angle. In [22], the authors propose using a problem-specific, user-defined threshold to determine whether a bend angle is sharp enough to classify the corresponding solution as a knee solution. If the threshold is set too high, a knee may not exist, and nondominated points that are practically significant may be excluded without proper fine-tuning of the threshold.

According to Branke et al. [9], utility-based methods identify knee solutions using a linear utility function of the form $U(F(x), \mu) = \sum_{i=1}^q \mu_i f_i(x)$, where μ lies in the simplex set. To identify a knee solution, one can assume a uniform distribution over the values of μ and maximize the expected value of a *marginal* utility function over a predetermined set of Pareto optimal solutions. For a given value of μ , the marginal utility of a Pareto optimal solution quantifies the loss in utility that would occur if such a solution were unavailable and the decision maker had to select the best remaining solution. In this sense, Pareto optimal solutions with high marginal utility are those whose removal would lead to a significant degradation in achievable utility, and are therefore interpreted as knee solutions; we refer to Branke et al. [9, Section 3.2] for the details. A variant of such a method is provided in Deb and Gupta [22, Definition 3], which defines a knee solution as a Pareto optimal solution that minimizes $U(F(\cdot), \mu)$ over a predetermined set of Pareto optimal solutions for the largest number of weight vectors μ chosen from the simplex set. Consequently, one must solve a minimization problem for each selected μ and count how often each Pareto optimal solution is obtained. The solution with the highest count is then defined as the knee solution.

Normal boundary intersection-based methods, applicable to an arbitrary number of objective func-

²In general, given q objectives, the corresponding Pareto front has at most q *extreme nondominated points* in the objective space, given by $F(x_*^i)$, where x_*^i is a minimizer of f_i , with $i \in \{1, \dots, q\}$.

tions, search for knee nondominated points on the Pareto front by maximizing their distance to the convex hull of the extreme points of the Pareto front, referred to as the boundary line. Such knee nondominated points are typically found in the intermediate region of the Pareto front (i.e., between the extreme nondominated points and away from the boundary of the front), especially when the front is convex [22]. To identify knee nondominated points and the corresponding knee solutions, one can employ a nonlinear constrained optimization approach, as introduced in [18] and [19], and further refined in [62]. Evolutionary algorithms were used to search for normal boundary intersection-based knee solutions in [74] and [5].

1.2 Computing knee solutions through Pareto sensitivity

As an advancement over existing multi-criteria decision-making techniques, the main contribution of our paper is the introduction of a novel approach for determining knee solutions and knee nondominated points through Pareto sensitivity. By Pareto sensitivity, we mean the application of sensitivity analysis principles to obtain a quantitative measure of how sensitive a Pareto optimal solution or a nondominated point is to variations in problem parameters. In our paper, such parameters correspond to the weights arising from the weighted-sum method (or to the right-hand side ε when using the ε -constraint method). We note that the study of sensitivity analysis in MOO dates back to the late 1980s [57, 67], where it was investigated through set-valued perturbation mappings and variational analysis frameworks, and has continued through more recent work [2]. None of these papers use the term *Pareto sensitivity*, which is introduced in our work to describe the use of sensitivity analysis techniques for characterizing Pareto optimal solutions and nondominated points. Related sensitivity techniques have recently gained attention in the bilevel and multilevel optimization literature, where they are used to compute the gradient of the objective function in the single-level reformulation of bilevel or trilevel problems [12, 31, 33, 34, 36, 40].

Consider the weighted-sum function associated with problem (1.1), $\sum_{i=1}^q \lambda_i f_i(x)$, where λ takes values in the simplex set Λ . Note that such a weighted-sum function can be interpreted as the linear utility function $U(F(x), \lambda)$ introduced in Subsection 1.1, with λ in place of μ . For each $\lambda \in \Lambda$, the minimization of the weighted-sum function over $x \in X$ leads to a Pareto optimal solution $x(\lambda)$. To define and determine a Pareto knee solution that follows the spirit of the verbal definition, for a given $\lambda \in \Lambda$, we propose using the maximum ratio $\|\nabla_{\lambda}(f_i(x(\lambda)))\|/\|\nabla_{\lambda}(f_j(x(\lambda)))\|$ of the norms of $\nabla_{\lambda}(f_i(x(\lambda)))$ and $\nabla_{\lambda}(f_j(x(\lambda)))$ ³ across all pairs of objective functions i and j , where $\{i, j\} \subseteq \{1, \dots, q\}$, with $i \neq j$. Such a ratio (which we refer to as the *maximal-change* function) measures the maximum change on the Pareto front around the nondominated point corresponding to the Pareto optimal solution $x(\lambda)$. Our knee solutions are identified by minimizing such a maximal-change function over λ in Λ , which leads to Pareto optimal solutions where the least maximal change on the Pareto front occurs (these concepts are described more formally in Section 3). When such a knee solution is selected, the decision maker is guaranteed that trading among objectives is optimally balanced, minimizing the extent of compromise required for one objective relative to the others. We refer to the resulting approach as the *sensitivity knee* (snee) approach. We note that the techniques used in our *snee* approach require the computation or approximations of first- and second-order derivatives and are still restricted to scalarized methods, in particular to the weighted-sum method considered in this paper.

Our *snee* approach provides a formal, quantitative definition for knee solutions that captures the essence of the verbal definition (see Definition 4 in Section 3). Since the maximal-change function that we minimize to identify a knee solution may be non-convex (regardless of the convexity of the Pareto

³Specifically, $\nabla_{\lambda} f_i(x(\lambda))$ represents the sensitivity of the i -th objective function to variations in the weight vector λ . Formal derivations for the unconstrained and constrained cases are provided in Subsections 5 and 6, respectively.

front) and thus may have more than one local minimizer, our knee solutions may have a local or global nature. Moreover, our knee solutions may not necessarily correspond to nondominated points in the intermediate region of the Pareto front (we again emphasize that by intermediate region, we mean the set of nondominated points that do not lie on the boundary of the Pareto front). The concept of knee nondominated points outside the intermediate region was analyzed in Deb and Gupta [22, Section 5], where such points, located near or at the extreme points of the Pareto front, are referred to as *edge-knee*. However, the definition of an edge-knee nondominated point applies only to MOO problems with 2 objectives and depends on a problem-specific, user-defined parameter, whereas our approach overcomes such limitations.

Given $\lambda \in \Lambda$, let $x(\lambda)$ be the corresponding Pareto optimal solution obtained by minimizing the weighted-sum function $\sum_{i=1}^q \lambda_i f_i(x)$ over $x \in X$. We will also see in Section 4 of this paper that the Jacobian matrix of the vector function $F(x(\lambda))$ with respect to λ can be used to define a neighborhood of weight vectors around λ (analogously, a neighborhood of Pareto optimal solutions around $x(\lambda)$), where the objective functions f_i exhibit the greatest variation per unit change of the weights. Local most-changing Pareto sub-fronts can then be computed by mapping the weight vectors in such a neighborhood through $F(x(\lambda))$ to the objective space \mathbb{R}^q . Nondominated points on these sub-fronts are distributed along directions of maximum change on the Pareto front. Such sub-fronts can assist decision makers in locally exploring different trade-offs.

To derive Pareto sensitivity in a convenient way and calculate the gradient of $f_i(x(\lambda))$ with respect to λ , required by our *snee* approach, with $i \in \{1, \dots, q\}$, we focus on the first-order necessary conditions for minimizing the weighted-sum function $\sum_{i=1}^q \lambda_i f_i(x)$ over $x \in X$, given $\lambda \in \Lambda$. Under the assumptions needed for the application of the implicit function theorem (collected in Assumption 5.1 in Subsection 5.1 for the unconstrained case $X = \mathbb{R}^n$, and in Assumption 6.1 in Subsection 6.1 for the constrained case $X \subset \mathbb{R}^n$), the solution $x(\lambda)$ satisfying such conditions is unique. By applying the chain rule to the first-order necessary conditions, we will first characterize the Jacobian, or sensitivity matrix, $\nabla x(\lambda)^\top$, and then calculate the gradient of $f_i(x(\lambda))$ with respect to λ . All these steps will be formally described in Sections 5 and 6.

Several advantages are offered by our *snee* approach compared to existing techniques:

1. Change on the Pareto front is quantified using the most universal concept of rate of change, i.e., first-order derivatives, eliminating the need for problem-specific, user-defined parameters.
2. It offers the flexibility to compute knee solutions according to the verbal definition, but in a quantifiable and optimal form, searching the Pareto front for local or global knee solutions, without relying on an approximation of the front in advance.
3. It can be applied to any number q of objective functions.
4. It detects a knee solution in the intermediate region of the Pareto front only if the trade-off between improvement and deterioration in the objectives is significant enough. Otherwise, the knee solution may lie on the boundary of the Pareto front.
5. It does not involve bilevel or minimax formulations, and it allows for easy use of off-the-shelf software.
6. The approach also allows for the identification of most-changing Pareto sub-fronts of predefined size, rather than focusing on a single Pareto optimal solution.

Our paper is organized as follows. In Section 2, we present basic MOO definitions and facts that will be used throughout the paper. In Section 3, we introduce the *snee* approach by developing a single-objective formulation to define and determine Pareto knee solutions. In Section 4, we address how to compute most-changing Pareto sub-fronts around a nondominated point. In Sections 5 and 6, we introduce general assumptions for problem (1.1) and derive Pareto sensitivity formulas for the unconstrained case ($X = \mathbb{R}^n$) and the constrained case ($X \subset \mathbb{R}^n$), respectively, including numerical results that illustrate the benefits of our approach. Finally, we draw some concluding remarks and ideas for future work in Section 7.

All code was implemented in Python 3.12.7. The experimental results were obtained using a Dell Latitude 5520 with 16GB of RAM and an Intel(R) Core(TM) i7-1185G7 processor running at 3.00GHz. Throughout the paper, $\|\cdot\|$ denotes the Euclidean norm $\|\cdot\|_2$.

2 MOO background

Consistent with common conventions in the MOO literature [26, Table 1.2], we adopt the following notation. Let $y^1, y^2 \in \mathbb{R}^q$. We write $y^1 \leq y^2$ if $y_i^1 \leq y_i^2$ for all $i \in \{1, \dots, q\}$, with $y^1 \neq y^2$ (componentwise order), and $y^1 < y^2$ if $y_i^1 < y_i^2$ for all $i \in \{1, \dots, q\}$ (strict componentwise order). The image of the feasible set X under the vector-valued function F is denoted as $Y = F(X)$. Pareto optimal solutions (or efficient solutions) of problem (1.1) and the corresponding weakly versions are introduced in Definitions 1 and 2 below [26, p. 24, Definition 2.1, and p. 38, Definition 2.24, respectively].

Definition 1 *A feasible point $\hat{x} \in X$ is called Pareto optimal or efficient if there is no other $x \in X$ such that $F(x) \leq F(\hat{x})$. If \hat{x} is Pareto optimal, $F(\hat{x})$ is called nondominated point. If $x^1, x^2 \in X$ and $F(x^1) \leq F(x^2)$, we say x^1 dominates x^2 and $F(x^1)$ dominates $F(x^2)$. The set of all Pareto optimal solutions $\hat{x} \in X$ is denoted X_E and called the efficient set. The set of all nondominated points $\hat{y} = F(\hat{x}) \in Y$, where $\hat{x} \in X_E$, is denoted Y_N and called the nondominated set.*

Definition 2 *A feasible point $\hat{X} \in X$ is called weakly Pareto optimal or weakly efficient if there is no $x \in X$ such that $F(x) < F(\hat{x})$. The point $\hat{y} = F(\hat{x})$ is then called weakly nondominated. The weakly efficient and nondominated sets are denoted X_{wE} and Y_{wN} , respectively.*

To be consistent with a significant portion of the multi-objective optimization literature [20, 21, 22, 23, 63], we also refer to Y_N as the Pareto front, and we note that alternative terminology, such as Pareto set, is also used [71]. Note that from Definitions 1 and 2, it follows that $Y_N \subset Y_{wN}$ and $X_E \subset X_{wE}$ [26, p. 39, eqs. (2.16) and (2.17)], where Ehrgott uses a strict inclusion to emphasize that equality does not necessarily hold.

Definition 3 below, based on Ehrgott [26, Definition 2.22], defines ideal and nadir points, which are the points in the objective space associated with the best and worst possible values for all objectives, respectively. Such points can be used to define the denominator of the metric that we will introduce to assess how well a local Pareto sub-front aligns with the direction of maximum change on the Pareto front (see (4.3) in Section 4).

Definition 3 (Ideal and nadir points) *The ideal point $F^I \in \mathbb{R}^q$ is the vector whose i -th component is given by $F_i^I = \min_{x \in X} f_i(x) = \min_{y \in Y} y_i$, for all $i \in \{1, \dots, q\}$. The nadir point $F^N \in \mathbb{R}^q$ is the vector whose i -th component is given by $F_i^N = \max_{x \in X_E} f_i(x) = \max_{y \in Y_N} y_i$, for all $i \in \{1, \dots, q\}$.*

To compute Pareto optimal solutions, one can use scalarization techniques to reduce a multi-objective problem into a single-objective one and then apply classical optimization methods. One popular scalarization technique is the weighted-sum method [26, 50], which consists of weighting the objective functions

into a single objective $\sum_{i=1}^q \lambda_i f_i(x)$, where λ_i are non-negative weights. The resulting optimization problem is

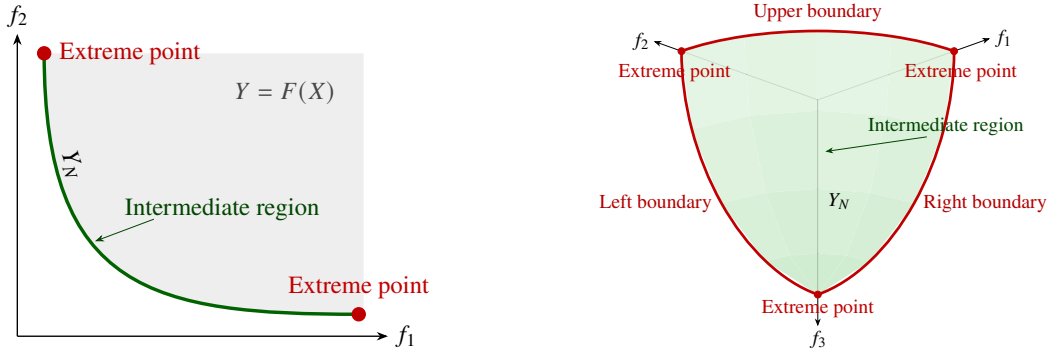
$$\min_{x \in X} \sum_{i=1}^q \lambda_i f_i(x). \quad (2.1)$$

We now present some properties of the weighted-sum method. Let Λ denote the simplex set, i.e.,

$$\Lambda = \{\lambda \in \mathbb{R}^q \mid \sum_{i=1}^q \lambda_i = 1, \lambda_i \geq 0, \forall i \in \{1, \dots, q\}\}.$$

It is well known that when X is a convex set and the objective functions f_1, \dots, f_q are convex, then $x_* \in X_{wE}$ if and only if there exists some weight vector $\lambda \in \Lambda$ such that x_* is an optimal solution to problem (2.1) [26, Propositions 3.9 and 3.10]. Moreover, if X is a convex set and the objective functions f_1, \dots, f_q are strictly convex, then $X_{wE} = X_E$ (the proof follows from basic facts and is omitted for brevity).

Finally, we briefly introduce the geometric concepts that we will use to describe the Pareto front Y_N . Under the settings considered in this paper, in the bi-objective case ($q = 2$), the front is a curve in \mathbb{R}^2 , and its boundary consists of two extreme nondominated points. In the tri-objective case ($q = 3$), the front is a two-dimensional surface in \mathbb{R}^3 , its boundary is formed by edge curves, and the intersections of two or more edge curves identify the extreme nondominated points. Following the terminology of Deb and Gupta [22], we define the *intermediate region* of the Pareto front as the set of nondominated points that do not lie on its boundary. Figure 1 illustrates these concepts for the bi-objective and tri-objective cases, respectively.



(a) Example of a Pareto front for a bi-objective problem ($q = 2$) (b) Example of a Pareto front for a tri-objective problem ($q = 3$)

Figure 1: Pareto fronts Y_N for a minimization problem in the bi-objective ($q = 2$, left) and tri-objective ($q = 3$, right) cases. The intermediate region comprises all nondominated points that are not on the boundary.

3 Finding knee solutions using Pareto sensitivity

In this section, we develop a single-objective optimization formulation to define and determine knee solutions and knee nondominated points. We begin by motivating our approach. When $q = 2$, a Pareto front can be modeled in the objective space as either the curve $f_2 = f_2(f_1)$ or the curve $f_1 = f_1(f_2)$. Let df_2/df_1 and df_1/df_2 denote the derivatives of f_2 with respect to f_1 and vice versa. These derivatives represent the slope of the tangent line to the corresponding curve at a given nondominated point. For

illustrative purposes, assume that df_2/df_1 and df_1/df_2 exist, meaning that we focus on nondominated points where the Pareto front curve is locally differentiable, without kinks or other singularities, and we exclude boundary points where the curve has vertical or horizontal tangents. In Deb and Gupta [22, Section 6], the authors note that according to the verbal definition (trade-off between improvement and deterioration in the objectives), knee solutions correspond to nondominated points where the derivatives df_2/df_1 and df_1/df_2 are equal in size. We then observe that a knee solution for $q = 2$ minimizes $\max\{|df_2/df_1|, |df_1/df_2|\}$. When $q > 2$, such an approach can be extended by minimizing the maximum $|df_i/df_j|$ for all pairs $\{i, j\} \subseteq \{1, \dots, q\}$, with $i \neq j$, in an attempt to levelize all the derivative sizes. However, such an approach is limited in practice by the fact that it would require the calculation of the entire Pareto front followed by the calculation of a model of the curves $f_i(f_j)$ to compute the derivatives df_i/df_j .

To replicate the role of $|df_i/df_j|$ without computing the entire Pareto front in advance, our *snee* approach uses the ratio between the norms of $\nabla_\lambda(f_i(x(\lambda)))$ and $\nabla_\lambda(f_j(x(\lambda)))$, resulting in the following maximal-change function (MCF):

$$\text{MCF}(\lambda) = \max_{\substack{\{i,j\} \subseteq \{1,\dots,q\} \\ i \neq j}} \frac{\|\nabla_\lambda(f_i(x(\lambda)))\|}{\|\nabla_\lambda(f_j(x(\lambda)))\|}. \quad (3.1)$$

Note that (3.1) is a function of λ . To determine the weight vector corresponding to a knee solution, we solve the following minimization problem:

$$\min_{\lambda \in \Lambda} \text{MCF}(\lambda). \quad (3.2)$$

Intuitively, the minimization problem in (3.2) aims to make the norms of $\nabla_\lambda(f_i(x(\lambda)))$ and $\nabla_\lambda(f_j(x(\lambda)))$ as close as possible⁴. Therefore, recalling that derivatives measure the rate of change of a function, our *snee* approach defines a knee solution as a Pareto optimal solution where the least maximal change of the Pareto front occurs (see Definition 4 below).

Definition 4 A Pareto knee solution is a Pareto optimal solution $x(\lambda_*)$ corresponding to an optimal solution λ_* of problem (3.2). The associated nondominated point $F(x(\lambda_*))$ in the objective space is called a knee nondominated point.

When selecting such a knee solution, the decision maker is thus protected against large trade-offs in a certain optimal way. Numerically, to avoid division by zero, we recommend replacing $\|\nabla_\lambda(f_j(x(\lambda)))\|$ in (3.1) by $\max\{\|\nabla_\lambda(f_j(x(\lambda)))\|, \text{eps}\}$, where *eps* represents the machine precision.

The procedure for determining a Pareto knee solution and its corresponding knee nondominated point via our *snee* approach is summarized in Algorithm 1. The main step in the procedure consists of solving problem (3.2), which involves the minimization of a non-smooth and non-convex function whose subgradients involve third-order derivatives. Note that the dimension of the problem is equal to the number q of objective functions, typically very low, and so problem (3.2) can be efficiently solved by a derivative-free optimization (DFO) algorithm [3, 16, 17, 44]. For instance, one may use two popular DFO algorithms: Nelder-Mead⁵ [52] and DIRECT⁶ [41]. Note that DFO is a well-studied class

⁴Hence, one could consider alternative formulations of (3.2), such as minimize the absolute value of the difference between the norms of $\nabla_\lambda(f_i(x(\lambda)))$ and $\nabla_\lambda(f_j(x(\lambda)))$.

⁵The Nelder-Mead (NM) algorithm uses a simplex of points to navigate the search space, adjusting the simplex through operations such as reflection, expansion, contraction, and shrinkage. It requires an initial starting point, but it typically involves fewer function evaluations than global methods like DIRECT, making it suitable for problems where computational efficiency is a priority.

⁶The DIRECT algorithm is a global optimization method that systematically divides the search space into hyper-rectangles,

of optimization methods. In the literature, it is also referred to as zeroth-order optimization [54] or black-box optimization [3].

Algorithm 1 Pareto Knee Solution Search

Input: Initial weight vector λ_0 .

Main step. Starting from λ_0 , solve problem (3.2) using a DFO algorithm to obtain λ_* . To evaluate the MCF (3.1) at each iteration of the DFO algorithm for a given $\lambda \in \Lambda$, perform these steps:

Step A. Given $\lambda \in \Lambda$, apply the weighted-sum method with weight vector λ to obtain $x(\lambda)$ by solving problem (2.1).

Step B. Given $x(\lambda)$ from **Step A**, compute the matrix $\nabla_\lambda(F(x(\lambda)))$ using (5.3) in Subsection 5.1 for the unconstrained case ($X = \mathbb{R}^n$) or (6.7) in Subsection 6.1 for the constrained case ($X \subset \mathbb{R}^n$).

Step C. Evaluate the MCF (3.1), where the gradients $\nabla_\lambda(f_i(x(\lambda)))$ and $\nabla_\lambda(f_j(x(\lambda)))$ correspond to the i -th and j -th columns of matrix $\nabla_\lambda(F(x(\lambda)))$ from **Step B**, respectively.

Output: Optimal weight vector λ_* and corresponding Pareto knee solution $x(\lambda_*)$.

To evaluate the MCF (3.1) at each iteration of the selected DFO algorithm for a given $\lambda \in \Lambda$, one first applies the weighted-sum method to obtain $x(\lambda)$ (**Step A**), and then computes the matrix $\nabla_\lambda(F(x(\lambda)))$ (**Step B**). Such a matrix is formally derived in (5.3) in Subsection 5.1 for the unconstrained case ($X = \mathbb{R}^n$) and (6.7) in Subsection 6.1 for the constrained case ($X \subset \mathbb{R}^n$). The MCF (3.1) is then evaluated by noting that the gradients $\nabla_\lambda(f_i(x(\lambda)))$ and $\nabla_\lambda(f_j(x(\lambda)))$ correspond to the columns of such a matrix (**Step C**).

Although using a DFO algorithm avoids the need for derivatives of the objective function in problem (3.2), one still needs to compute the gradients in (3.1) to evaluate the MCF. For large-scale machine learning applications, this may require using stochastic gradients (see Remark 3.1 below).

Remark 3.1 *Even when using a DFO algorithm, we need to efficiently compute the gradients required in (3.1) to evaluate the MCM function. In machine learning applications, where computing a gradient involves summing the loss over the entire dataset, researchers typically use a stochastic gradient computed from a randomly sampled subset of data [8, 15, 58, 60]. When the gradients $\nabla_\lambda(f_i(x(\lambda)))$ and $\nabla_\lambda(f_j(x(\lambda)))$ in (3.1) are approximated via stochastic gradients, the objective function of problem (3.2) should include an expectation over the probability distribution used to sample the data, introducing additional challenges that are beyond the scope of this paper. Moreover, note that many popular loss functions in machine learning are nonconvex (see Bottou et al. [8, Subsection 4.3]) and therefore do not satisfy Assumptions 5.1 and 6.1, which will be introduced in Subsections 5.1 and 6.1. Finally, we note that our approach requires solving the weighted-sum problem (2.1) for each λ generated by a DFO algorithm (see **Step A** of Algorithm 1). This may be computationally expensive when the weighted-sum problem is difficult to solve. In such cases, the normal boundary intersection method can be preferable because it requires solving only a single nonlinear constrained optimization problem, provided that extreme nondominated points (or estimates thereof) of the Pareto front are available.*

calculating objective function values to find potential global minima without requiring derivative information. It does not require an initial starting point and it may necessitate a substantial number of function evaluations.

4 Most-changing Pareto sub-fronts around nondominated points

Given a Pareto optimal solution x_c of interest, we want to find a neighborhood of Pareto optimal solutions around x_c where the objective functions in F change the most. In this paper, we will address this question in the space of weight vectors, and thus we seek a neighborhood of weight vectors λ centered at λ_c , with $x_c = x(\lambda_c)$, where $F(x(\lambda))$ changes the most. The resulting Pareto sub-front consists of the nondominated points corresponding to the Pareto optimal solutions identified by weight vectors in the neighborhood of λ_c . It can optionally be computed from the λ_* produced by Algorithm 1 in Section 3, with $\lambda_c = \lambda_*$, to visually highlight points along the direction of maximum change on the Pareto front around the knee nondominated point $F(x(\lambda_*))$. Next, we detail how to construct such a Pareto sub-front.

Given a neighborhood size $\alpha > 0$, a sub-front of most change is identified using the following neighborhood of weight vectors

$$\mathcal{E}_\alpha(\lambda_c) = \{\lambda \in \mathbb{R}^q \mid \|\nabla_\lambda(F(x(\lambda_c)))^\dagger(\lambda - \lambda_c)\| \leq \alpha\}, \quad (4.1)$$

where $\nabla_\lambda(F(x(\lambda_c)))$ is the transpose of the Jacobian matrix of $F(x(\cdot))$ evaluated at λ_c , and $\nabla_\lambda(F(x(\lambda_c)))^\dagger$ is its pseudo-inverse. Neighborhood (4.1) can be motivated in two different, related ways. First note that when $n = q = 1$, we obtain $|\lambda - \lambda_c| \leq \alpha \cdot \frac{d}{d\lambda}(f(x(\lambda_c)))$, where $\frac{d}{d\lambda}(f(x(\lambda_c)))$ denotes the derivative of $f(x(\cdot))$ evaluated at λ_c , and we can see that we are basically considering larger intervals centered at λ_c with amplitudes increasing with the slope. This observation provides a geometric interpretation of (4.1), as the resulting neighborhood is an ellipsoid with its major axis aligned with the direction of maximum change. For the remainder of the paper, we refer to neighborhood (4.1) as the ellipsoidal neighborhood.

One can also introduce a motivating argument based on the general notion of steepest ascent/descent. We are interested in the weight vectors λ that lead to a meaningful change in $\|F(x(\lambda)) - F(x(\lambda_c))\|$. Given the expansion

$$\|F(x(\lambda)) - F(x(\lambda_c))\| = \|\nabla_\lambda(F(x(\lambda_c)))\Delta\lambda\| + \mathcal{O}(\|\Delta\lambda\|^2),$$

we ask for a quadratic decrease in $\|\lambda - \lambda_c\|$ and introduce the neighborhood

$$\mathcal{E}_\beta(\lambda_c) = \{\lambda \in \mathbb{R}^q \mid \|\nabla_\lambda(F(x(\lambda_c)))\Delta\lambda\| \geq \beta\|\lambda - \lambda_c\|^2\}, \quad (4.2)$$

for some $\beta > 0$. Note that $\|\nabla_\lambda(F(x(\lambda_c)))\Delta\lambda\| \geq \beta\|\lambda - \lambda_c\|^2$ implies

$$\frac{\kappa(\nabla_\lambda(F(x(\lambda_c))))}{\beta} \geq \|\nabla_\lambda(F(x(\lambda_c)))^\dagger(\lambda - \lambda_c)\|,$$

where $\kappa(\nabla_\lambda(F(x(\lambda_c)))) = \|\nabla_\lambda(F(x(\lambda_c)))\| \|\nabla_\lambda(F(x(\lambda_c)))^\dagger\|$ measures the conditioning of $\nabla_\lambda(F(x(\lambda_c)))$ beyond singularity. We conclude that for moderate $\kappa(\nabla_\lambda(F(x(\lambda_c))))$, we recover (4.1) from (4.2) by setting $\alpha = \kappa(\nabla_\lambda(F(x(\lambda_c))))/\beta$. Geometrically, neighborhood (4.2) has a shape similar to a Cassini oval [45, p. 153], which is visible in some of the plots of this paper. For reference, a Cassini oval is the set of points in the plane such that the product of the distances to two fixed points (foci) is constant. Neighborhood (4.2) only roughly resembles this shape.

Given a weight vector λ_c , to evaluate the effectiveness of a Pareto neighborhood $\mathcal{E}(\lambda_c)$ —either $\mathcal{E}_\alpha(\lambda_c)$ in (4.1) or $\mathcal{E}_\beta(\lambda_c)$ in (4.2)—in identifying the greatest variation across the objectives on the Pareto front through the corresponding Pareto sub-front $\{F(x(\lambda)) \mid \lambda \in \mathcal{E}(\lambda_c)\}$, we will use the most-changing metric (4.3) below. Such a metric measures the extent of the Pareto front covered by a set of nondominated points relative to the full extent of the front. In the literature, such a metric is referred to as the overall

Pareto spread [4, 72]. In our paper, we prefer not to use the term *spread* because it is not relevant to our context. The most-changing metric (4.3) evaluates the extent of the Pareto front covered by the nondominated points corresponding to the Pareto optimal solutions obtained by applying the weighted-sum method with weight vectors in the intersection between a Pareto neighborhood and the simplex set. In particular, the most-changing metric (MCM) is given by

$$\text{MCM} = \text{MCM}(\mathcal{E}(\lambda_c)) = \prod_{i=1}^q \frac{|\max_{\lambda \in \mathcal{E}(\lambda_c) \cap \Lambda} f_i(x(\lambda)) - \min_{\lambda \in \mathcal{E}(\lambda_c) \cap \Lambda} f_i(x(\lambda))|}{|\max_{\lambda \in \Lambda} f_i(x(\lambda)) - \min_{\lambda \in \Lambda} f_i(x(\lambda))|}. \quad (4.3)$$

The numerator in (4.3) measures the maximum variation of the objective function f_i over the set of weights in $\mathcal{E}(\lambda_c) \cap \Lambda$. The denominator measures the maximum variation of f_i over the set of weights in Λ . The denominator can also be written as $|F_i^I - F_i^N|$, where F^I and F^N are the ideal and nadir points introduced in Definition 3 in Section 2. Note that metric (4.3) lies between 0 and 1. Since such a metric is computed relative to the full Pareto front, it is not affected by differences in the orders of magnitude of the objective functions. A higher value of metric (4.3) indicates that the corresponding Pareto sub-front exhibits greater variation across the objectives.

To determine the values of α and β in neighborhoods (4.1) and (4.2), one can use either a fixed stepsize or an adaptive rule. Using a fixed value requires fine-tuning and may be unreliable, as observed in the numerical experiments (see Remark 5.1 in Subsection 5.3). To apply the proposed adaptive rule, we consider a finite set of equidistant weight vectors corresponding to a fine-scale discretization of Λ , i.e., $\Lambda_m = \{\lambda_1, \dots, \lambda_m\} \subset \Lambda$. Specifically, for neighborhood (4.1), we set α to $\gamma(1/m) \sum_{i=1}^m \|\nabla_{\lambda}(F(x(\lambda_c)))^{\dagger}(\lambda_i - \lambda_c)\|$, where $\gamma > 0$. The value of γ should be chosen so that a reasonable proportion of the weight vectors in Λ_m lie within each neighborhood $\mathcal{E}(\lambda_c)$. A similar adaptive rule can be applied for neighborhood (4.2).

The next remark gives insights into how to determine a most-changing Pareto sub-front when multiple nondominated points are available.

Remark 4.1 *If one wants to determine a most-changing Pareto sub-front around multiple nondominated points, there are several approaches one can use based on the above procedure for a single point. A first approach consists of computing a most-changing neighborhood using the centroid of the weight vectors that correspond to the given nondominated points. A second approach involves determining the centroid of the given nondominated points and computing a most-changing neighborhood using a matrix that could be either the Jacobian at the centroid or a linear combination of the Jacobians at the given nondominated points. A third approach consists of computing a most-changing Pareto sub-front for all the given nondominated points, and then taking the union of such sub-fronts.*

5 The unconstrained case

Throughout this section, we focus on the case $X = \mathbb{R}^n$.

5.1 Pareto sensitivity calculation in the unconstrained case

In this subsection, given $\lambda \in \Lambda$, we first characterize the Jacobian, or sensitivity matrix, $\nabla_x(\lambda)^{\top}$, and then calculate the gradient of $f_i(x(\lambda))$ with respect to λ , for all $i \in \{1, \dots, q\}$. Such a gradient allows us to derive the Jacobian matrix of $F(x(\lambda)) = (f_1(x(\lambda)), \dots, f_q(x(\lambda)))^{\top}$ with respect to λ , which plays a crucial role in determining Pareto knee solutions in Section 3 and in computing Pareto sub-fronts in Section 4.

For any given $\lambda \in \Lambda$, let us assume the existence of $x(\lambda)$ satisfying the first-order necessary optimality conditions

$$\sum_{i=1}^q \lambda_i \nabla_x f_i(x(\lambda)) = 0. \quad (5.1)$$

We will later collect all the assumptions required for the application of the implicit function theorem at $x(\lambda)$ (i.e., Assumption 5.1 below), which ensures the uniqueness of $x(\lambda)$ and its continuous differentiability [59, p. 224, Theorem 9.28]. To calculate the Jacobian $\nabla x(\lambda)^\top \in \mathbb{R}^{n \times q}$, we take derivatives with respect to λ on both sides of the first-order necessary optimality conditions (5.1), obtaining

$$(\nabla_x f_1(x(\lambda)), \dots, \nabla_x f_q(x(\lambda)))^\top + \sum_{i=1}^q \lambda_i \nabla x(\lambda) \nabla_{xx}^2 f_i(x(\lambda)) = 0,$$

which, under appropriate assumptions, yields

$$\nabla x(\lambda) = -(\nabla_x f_1(x(\lambda)), \dots, \nabla_x f_q(x(\lambda)))^\top \left(\sum_{i=1}^q \lambda_i \nabla_{xx}^2 f_i(x(\lambda)) \right)^{-1}. \quad (5.2)$$

By applying the chain rule and using (5.2), the transpose of the Jacobian matrix of $F(x(\cdot))$ at λ is given by

$$\begin{aligned} \nabla_\lambda(F(x(\lambda))) &= \nabla x(\lambda) \nabla_x F(x(\lambda)) \\ &= -(\nabla_x f_1, \dots, \nabla_x f_q)^\top \left(\sum_{i=1}^q \lambda_i \nabla_{xx}^2 f_i \right)^{-1} (\nabla_x f_1, \dots, \nabla_x f_q), \end{aligned} \quad (5.3)$$

where all the gradients $\nabla_x f_i$ and Hessians $\nabla_{xx}^2 f_i$ are evaluated at $x(\lambda)$, with $i \in \{1, \dots, q\}$. Recalling that $F(x(\lambda)) = (f_1(x(\lambda)), \dots, f_q(x(\lambda)))^\top$, the columns of $\nabla_\lambda(F(x(\lambda)))$ correspond to the gradients of the functions $f_i(x(\lambda))$, i.e., $\nabla_\lambda(F(x(\lambda))) = (\nabla_\lambda(f_1(x(\lambda))), \dots, \nabla_\lambda(f_q(x(\lambda))))^\top$. Note that $\nabla_\lambda(F(x(\lambda)))$ is symmetric. It is also singular due to the fact that (5.1) implies the linear dependence of the gradients at $x(\lambda_c)$.

To apply this derivation when $X = \mathbb{R}^n$, we have required the matrix resulting from the convex linear combination of the individual Hessian matrices to be non-singular at $x(\lambda)$, as evident from the expression for $\nabla_\lambda(F(x(\lambda)))$ in (5.3). We collect all the required working assumptions in Assumption 5.1 below. Note that a sufficient condition for Assumption 5.1 to hold is that the objective functions f_1, \dots, f_q are strongly convex [53, p. 74, Definition 2.1.3]. In this case, for any $\lambda \in \Lambda$, the weighted-sum function $\sum_{i=1}^q \lambda_i f_i(x)$ has a unique minimizer $x(\lambda)$ and the Hessian $\sum_{i=1}^q \lambda_i \nabla_{xx}^2 f_i(x(\lambda))$ is positive definite and therefore nonsingular [53, p. 75, Theorem 2.1.11].

Assumption 5.1 (Existence of Pareto optimal solutions (LL unconstrained case)) *Let $X = \mathbb{R}^n$. The objective functions f_1, \dots, f_q are twice continuously differentiable. For any $\lambda \in \Lambda$, there exists a point $x(\lambda)$ such that $\sum_{i=1}^q \lambda_i \nabla_x f_i(x(\lambda)) = 0$ and the convex linear combination $\sum_{i=1}^q \lambda_i \nabla_{xx}^2 f_i(x(\lambda))$ of the individual Hessian matrices is non-singular.*

Note that if we are given a Pareto optimal solution x_c , and the objective functions meet the conditions of Assumption 5.1, one can calculate a λ_c such that the first-order necessary conditions (5.1) are satisfied, and then proceed from there to calculate a sub-front of most change. Note also that such a λ_c may not be unique, which could potentially lead to different sub-fronts of most change (see Example 5.1 below).

Problem	n	q	Ref.	Objective Functions
ZLT1	3	3	[38]	$f_1(x_1, x_2, x_3) = (x_1 - 1)^2 + x_2^2 + x_3^2$ $f_2(x_1, x_2, x_3) = x_1^2 + (x_2 - 1)^2 + x_3^2$ $f_3(x_1, x_2, x_3) = x_1^2 + x_2^2 + (x_3 - 1)^2$
GRV1	$2\bar{n}$	3		$f_1(x_1, x_2) = \frac{1}{2}x_1^\top H_1 x_1 + \frac{1}{2}x_2^\top H_2 x_2 + x_1^\top H_3 x_2 + a_1^\top x_1 + a_2^\top x_2$ $f_2(x_1, x_2) = \frac{1}{2}x_1^\top H_3 x_1 + \frac{1}{2}x_2^\top H_4 x_2 + x_1^\top H_5 x_2 + a_3^\top x_1 + a_4^\top x_2$ $f_3(x_1, x_2) = \frac{1}{2}x_1^\top H_7 x_1 + \frac{1}{2}x_2^\top H_8 x_2 + x_1^\top H_9 x_2 + a_5^\top x_1 + a_6^\top x_2$
VFM1	2	3	[38]	$f_1(x_1, x_2) = x_1^2 + (x_2 - 1)^2$ $f_2(x_1, x_2) = x_1^2 + (x_2 + 1)^2 + 1$ $f_3(x_1, x_2) = (x_1 - 1)^2 + x_2^2 + 2$
ZLT1 q	\bar{n}	\bar{q}	[38]	$f_j(x) = (x_j - 1)^2 + \sum_{1 \leq i \leq \bar{n}, i \neq j} x_i^2, \quad j \in \{1, \dots, \bar{q}\}$
GRV2	\bar{n}	2		$f_1(x) = \frac{1}{\bar{n}} \sum_{i=1}^{\bar{n}} x_i^2 + \frac{1}{2} \sum_{i=1}^{\bar{n}} x_i^4$ $f_2(x) = \frac{1}{\bar{n}} \sum_{i=1}^{\bar{n}} (x_i - 2)^2 + \frac{1}{2} \sum_{i=1}^{\bar{n}} (x_i - 2)^4$

Table 1: Unconstrained test problems (\bar{n} and \bar{q} are arbitrary positive scalars).

Example 5.1 Consider $n = 1$, $q = 3$ with $f_1(x) = (x - 1)^2$, $f_2(x) = x^2$, $f_3(x) = (x + 1)^2$. Each f_i has Hessian $f_i''(x) = 2 > 0$, so all three objectives are strongly convex and Assumption 1 holds. The first-order necessary optimal conditions (5.1) reduce to $\sum_{i=1}^3 \lambda_i f_i'(x) = 0$, which gives $x(\lambda) = \lambda_1 - \lambda_3$. Now, choose arbitrarily $x_c = 0.2$. The condition $\lambda_1 - \lambda_3 = 0.2$ together with $\lambda_1 + \lambda_2 + \lambda_3 = 1$ and $\lambda_i \geq 0$ admits the one-parameter family $\lambda_c(t) = (0.2 + t, 0.8 - 2t, t)^\top$, $t \in [0, 0.4]$, so infinitely many weight vectors correspond to the same x_c . Three members of this family are $\lambda_c^{(1)} = (0.2, 0.8, 0)^\top$, $\lambda_c^{(2)} = (0.4, 0.4, 0.2)^\top$, and $\lambda_c^{(3)} = (0.6, 0, 0.4)^\top$. This illustrates the non-uniqueness of λ_c when $n < q - 1$ (here $n = 1$ and $q - 1 = 2$). Although all three weight vectors yield $x(\lambda_c) = 0.2$ and produce the same $\nabla_\lambda(F(x(\lambda_c)))$ (since it depends on λ only through $x(\lambda_c)$), neighborhoods (4.1) and (4.2) are centered at different vectors, so the corresponding Pareto sub-fronts will generally differ across choices of λ_c .

5.2 MOO unconstrained test problems

Table 1 specifies the unconstrained test problems used for the experiments in Subsections 5.3 and 5.4, along with the number of variables and objectives (i.e., n and q , respectively). All of the problems have strictly convex objective functions. In Problem GRV1, a_1 , a_2 , and a_5 were randomly generated according to a uniform distribution over $[-5, 0)$, resulting in $a_1 = -1.87$, $a_2 = -4.75$, and $a_5 = -0.78$. Similarly, a_3 , a_4 , and a_6 were randomly generated according to a uniform distribution over $[0, 5)$, resulting in $a_3 = 3.66$, $a_4 = 2.99$, and $a_6 = 0.78$. Additionally, we randomly generated three $\bar{n} \times \bar{n}$ symmetric positive definite matrices $H^{(1)}$, $H^{(2)}$, and $H^{(3)}$, and we set the matrices in the objective functions f_i , with $i \in \{1, 2, 3\}$, as follows:

$$H^{(1)} = \begin{bmatrix} H_1 & H_3 \\ H_3^\top & H_2 \end{bmatrix} = \begin{bmatrix} 50.82 & -0.23 \\ -0.23 & 10.57 \end{bmatrix}, \quad H^{(2)} = \begin{bmatrix} H_4 & H_6 \\ H_6^\top & H_5 \end{bmatrix} = \begin{bmatrix} 38.25 & 12.19 \\ 12.19 & 6.53 \end{bmatrix},$$

$$H^{(3)} = \begin{bmatrix} H_7 & H_9 \\ H_9^\top & H_8 \end{bmatrix} = \begin{bmatrix} 45.10 & -9.55 \\ -9.55 & 9.91 \end{bmatrix}.$$

5.3 Results for knee solutions using Pareto sensitivity in the unconstrained case

We consider the unconstrained problems from Table 1 in Subsection 5.2. For each problem with $n \leq 3$ and $q \leq 3$, we graphically represent the weight vector, objective, and decision spaces. To solve

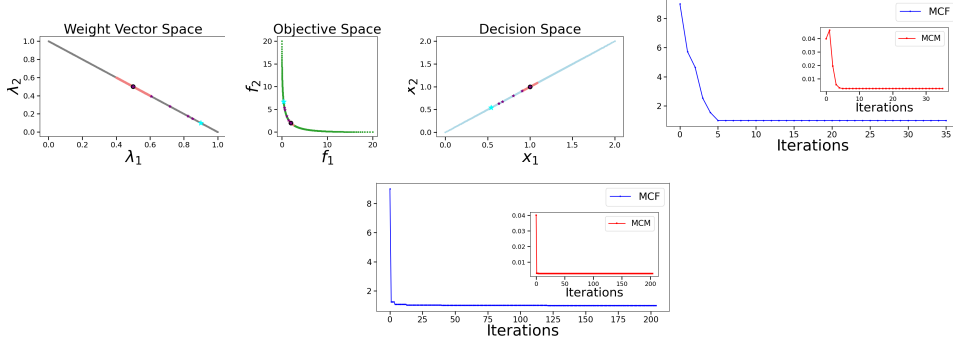


Figure 2: Results for problem GRV2 (for \bar{n} in Table 1 equal to 2). The three leftmost plots show the weight vector, objective, and decision spaces, respectively, when applying the NM algorithm in the main step of Algorithm 1, including the iterates of the optimization process, the neighborhood of weight vectors, the Pareto sub-front centered at the knee nondominated point, and the neighborhood of Pareto optimal solutions centered at the knee solution. The two rightmost plots show the values of the MCF and MCM over the iterations (left: NM, right: DIRECT).

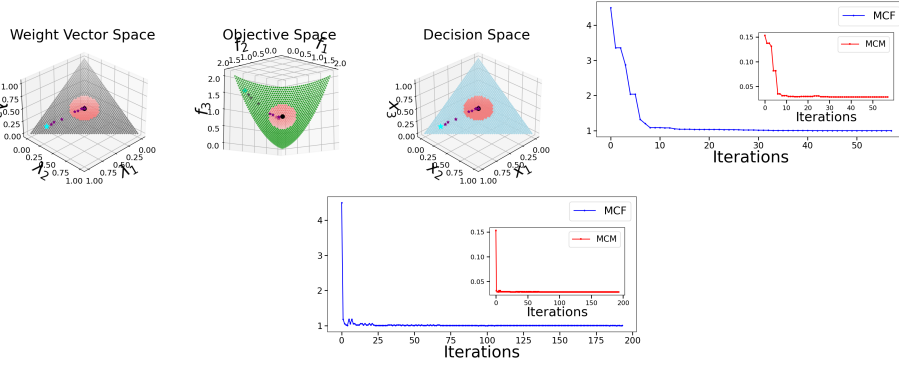


Figure 3: Results for problem ZLT1. See the caption of Figure 2 for details.

problem (3.2) in the main step of Algorithm 1, we employ both the NM and DIRECT methods introduced in Section 3. Specifically, we use the implementations available in the Python SciPy library [69] with default parameters. At each iteration of both methods, feasibility is ensured by computing orthogonal projections onto Λ . To perform **Step A** and obtain the Pareto optimal solution associated with a given weight vector, we solve the weighted-sum problem (2.1) using the BFGS algorithm implementation available in the Python SciPy library [30, 69], again with default parameters.

Figure 2 presents the results for problem GRV2, while Figures 3–6 present the results for problems ZLT1, GRV1, VFM1, and ZLT1 q . When using the NM algorithm, the initial weight vector λ_0 in Algorithm 1 is set arbitrarily as follows: for problem GRV2, $\lambda_0 = (0.9, 0.1)$; for problems ZLT1 and GRV1, $\lambda_0 = (0.8, 0.1, 0.1)$; and for problems VFM1 and ZLT1 q , $\lambda_0 = (0.4, 0.2, 0.4)$ and $\lambda_0 = (0.6, 0.1, 0.1, 0.1, 0.1)$, respectively. In each figure, in the weight vector space, the iterates of the NM algorithm in the main step of Algorithm 1 are represented by purple stars, with the initial iterate indicated by a cyan star and the final one by a black dot. In the objective and decision spaces, the same color coding is used to represent the Pareto optimal solutions and nondominated points corresponding to such iterates. To avoid redundancy, we do not represent the weight vector, objective, and decision spaces for the DIRECT algorithm because its final solution to the minimization problem (3.2) in the main step

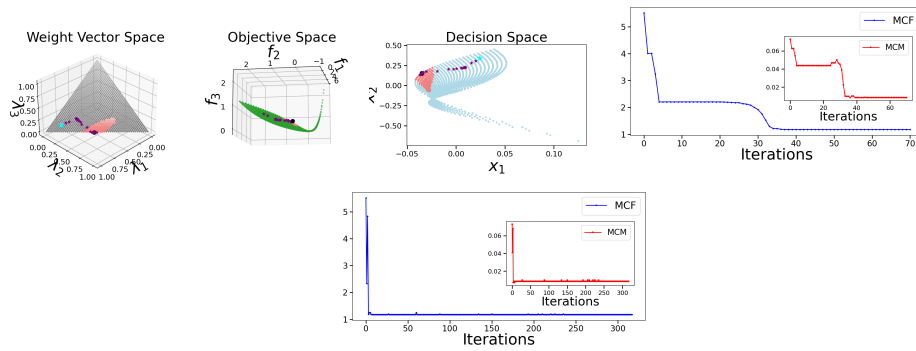


Figure 4: Results for problem GRV1 (for \bar{n} in Table 1 equal to 2). See the caption of Figure 2 for details.

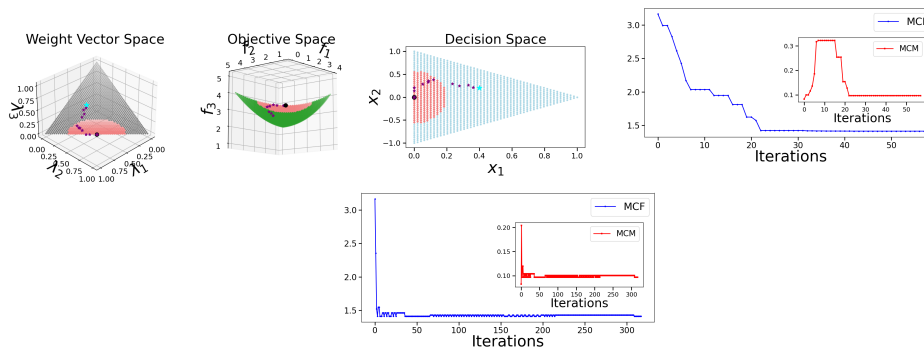


Figure 5: Results for problem VFM1. See the caption of Figure 2 for details.

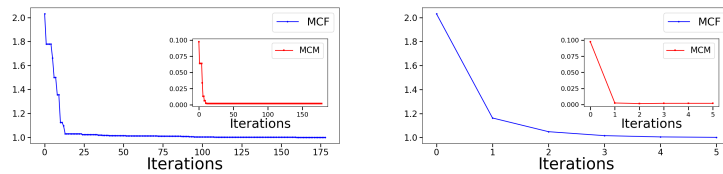


Figure 6: Results for problem ZLT1 q (for \bar{n} in Table 1 equal to 5). The plots show the values of the MCF and MCM over the iterations (left: NM, right: DIRECT).

of Algorithm 1 is nearly identical to that of the NM algorithm (there are no noticeable differences in the plots).

Each figure also includes plots that show the values of the MCF (3.1) over the iterations (the plot on the left corresponds to NM, while the plot on the right corresponds to DIRECT). One can observe that the NM and DIRECT algorithms achieve the same minimum values for the MCF.

Note that the knee nondominated points found by both the NM and DIRECT algorithms lie in the intermediate regions of the Pareto fronts, except for problem VFM1, where the knee nondominated point lies on the upper boundary of the Pareto front (see Figure 5). This outcome aligns with the concept of edge-knee nondominated points proposed in [22] for problems with 2 objectives, but differs from the knee nondominated points found by the normal boundary intersection method [18, 19], which tends to identify points in the intermediate region of a Pareto front (when it is convex), depending on where the distance between a point on the front and the convex hull of the extreme points is maximized. If the front lacks a bulge (i.e., a region where a small improvement in any objective leads to a large deterioration in at least one other objective, which is the verbal definition of a knee solution), the point found by our approach will not be in the intermediate region, as there is no clear knee nondominated point according to the verbal definition.

For the purpose of evaluating the MCM, we need to compute the local most-changing Pareto sub-fronts in the objective space. We visualize these sub-fronts along with the corresponding neighborhoods of weight vectors and Pareto optimal solutions in the weight vector and decision spaces, respectively. The neighborhoods of weight vectors shown in the figures are the ellipsoidal ones, centered at the best iterate returned by the NM algorithm. For such neighborhoods, the size α is set to 0.1 for all problems, except for GRV2, where using a fixed neighborhood size results in ellipsoidal neighborhoods that either have no elements or contain the entire simplex set at certain iterations. Therefore, for GRV2, we determine the neighborhood size using the adaptive rule described in Section 4 with $\gamma = 0.4$, which ensures that approximately 40% of the weight vectors in the fine-scale discretization of Λ are included in the neighborhood at each iteration. The same adaptive rule will be used for the problems in Subsection 6.3.

One can observe from each figure that the MCM (4.3) is approximately correlated with the MCF. Note that the neighborhoods are required only for computing the MCM and not for the MCF. Remark 5.1 below explains that minimizing the MCF provides a more reliable approach than minimizing the MCM.

Remark 5.1 *Given the approximate correlation between the MCF and MCM, one might think that knee solutions could be obtained by minimizing the MCM over λ_c instead of the MCF over λ . However, such an approach presents challenges because $\text{MCM} = \text{MCM}(\mathcal{E}_\alpha(\lambda_c))$ depends on the neighborhood size α . With fixed right-hand sides, the MCM may achieve a small value for a neighborhood $\mathcal{E}(\lambda_c)$ with a small size (particularly in regions of the weight vector space where the norm of $\nabla_\lambda(F(x(\lambda_c)))$ is low), even if its center λ_c is not a knee solution. Therefore, minimizing the MCF provides a more reliable approach.*

5.4 Results for most-changing Pareto sub-fronts using Pareto sensitivity

We now perform numerical experiments to assess which neighborhood is more effective at identifying the greatest variation across the objectives on the Pareto front through the corresponding Pareto sub-front. We consider the neighborhood achieving the highest value of the MCM (4.3) to be the most effective. We again consider the problems from Table 1 in Subsection 5.2. In this section, we do not include results for problem GRV2, where $q = 2$, because both the ellipsoidal neighborhood $\mathcal{E}_\alpha(\lambda_c)$ in (4.1) and neighborhood $\mathcal{E}_\beta(\lambda_c)$ in (4.2) yield similar Pareto sub-fronts in the bi-objective case, providing little insight into our understanding of which one is more effective. We use the weight vectors λ_0 from

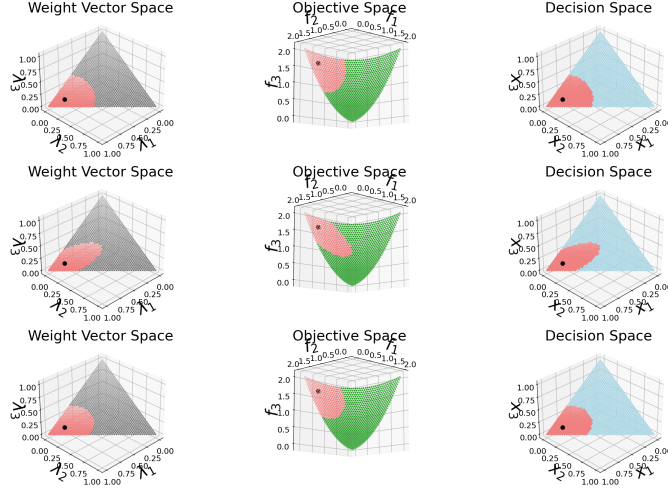


Figure 7: Results for problem ZLT1. In the weight vector space, we show the neighborhood of weight vectors centered at λ_c . In the objective and decision spaces, we show the Pareto sub-front centered at $F(x(\lambda))$ and neighborhood of Pareto optimal solutions centered at $x(\lambda)$, respectively. Upper, middle, and lower rows correspond to neighborhoods $\mathcal{B}_r(\lambda_c)$, $\mathcal{E}_\alpha(\lambda_c)$, and $\mathcal{E}_\beta(\lambda_c)$. The ellipsoidal neighborhood $\mathcal{E}_\alpha(\lambda_c)$ is the most effective at capturing the greatest variation across the objectives.

Subsection 5.3 as the neighborhood centers λ_c for problems ZLT1, GRV1, VFM1, and ZLT1 q . We compare both neighborhoods (4.1) and (4.2) against a ball of radius r , defined as follows

$$\mathcal{B}_r(\lambda_c) = \{\lambda \in \mathbb{R}^q \mid \|\lambda - \lambda_c\| \leq r\}. \quad (5.4)$$

Note from (4.1) and (5.4) that $\mathcal{B}_r(\lambda_c)$ is equal to $\mathcal{E}_\alpha(\lambda_c)$ when $r = \alpha$ and the Jacobian of $F(x(\cdot))$ is equal to the identity matrix. When using the ellipsoidal neighborhood $\mathcal{E}_\alpha(\lambda_c)$, we set α to 0.10, which results in neighborhoods that include roughly 10%-25% of the weight vectors in the fine-scale discretization of Λ , $\{\lambda_1, \dots, \lambda_m\} \subset \Lambda$, introduced in Subsection 5.3. In practice, the value of α should be chosen by a decision maker. When using $\mathcal{B}_r(\lambda_c)$ and $\mathcal{E}_\beta(\lambda_c)$, we set r and β to values that produce neighborhoods containing approximately the same percentage of weight vectors as $\mathcal{E}_\alpha(\lambda_c)$.

Figures 7–9 illustrate the results for problems ZLT1, GRV1, and VFM1. In each plot, the black dot represents the center of the corresponding neighborhood or sub-front. Such figures show that $\mathcal{E}_\alpha(\lambda_c)$ and $\mathcal{E}_\beta(\lambda_c)$ lead to sub-fronts where nondominated points are distributed along directions of maximum change of the Pareto front. The values of the MCM (4.3) for problems ZLT1, GRV1, VFM1, and ZLT1 q are included in Table 2 below for each type of neighborhood, along with the values of n and q used in the experiments and the fraction of the weight vectors in Λ_m that are contained within each neighborhood. Similar to Subsection 5.3, to obtain the Pareto optimal solutions associated with each weight vector in a neighborhood, we minimized the corresponding weighted-sum function using the BFGS algorithm implementation available in the Python SciPy library [30, 69], with default parameters. When computing the MCM for the ball (5.4), we replace $\mathcal{E}(\lambda_c)$ in (4.3) with $\mathcal{B}_r(\lambda_c)$.

From the MCM column of Table 2, one can observe that $\mathcal{E}_\alpha(\lambda_c)$ outperforms $\mathcal{E}_\beta(\lambda_c)$ and $\mathcal{B}_r(\lambda_c)$ on all of the problems, even though all neighborhoods are comparable in size (see the last column of Table 2). Additionally, $\mathcal{E}_\beta(\lambda_c)$ yields (nearly all the times) better results than $\mathcal{B}_r(\lambda_c)$.

6 The constrained case

Throughout this section, we focus on the case where X is not \mathbb{R}^n .

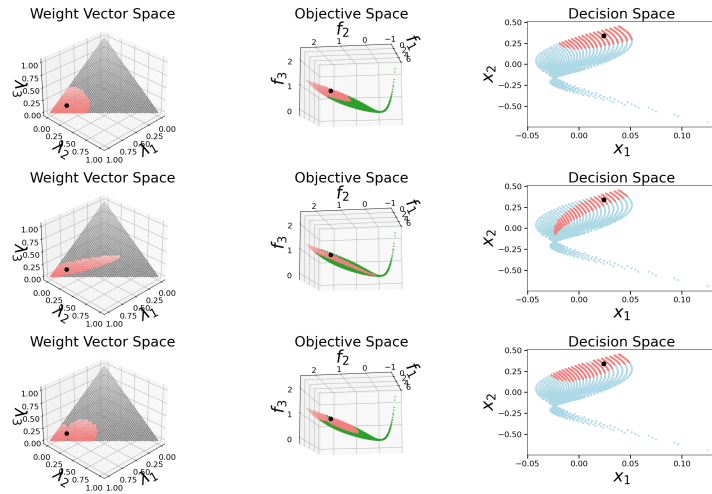


Figure 8: Results for problem GRV1 (for \bar{n} in Table 1 equal to 2). Upper, middle, and lower rows correspond to neighborhoods $\mathcal{B}_r(\lambda_c)$, $\mathcal{E}_\alpha(\lambda_c)$, and $\mathcal{E}_\beta(\lambda_c)$ (see the caption of Figure 7 for details). The ellipsoidal neighborhood $\mathcal{E}_\alpha(\lambda_c)$ is the most effective at capturing the greatest variation across the objectives.

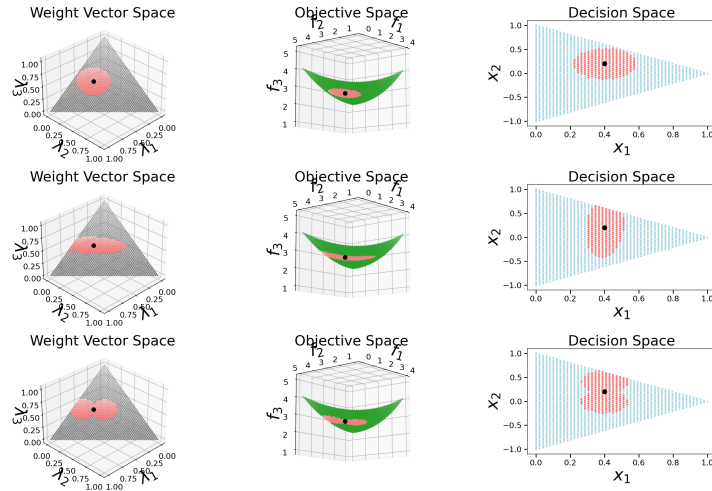


Figure 9: Results for problem VFM1. Upper, middle, and lower rows correspond to neighborhoods $\mathcal{B}_r(\lambda_c)$, $\mathcal{E}_\alpha(\lambda_c)$, and $\mathcal{E}_\beta(\lambda_c)$ (see the caption of Figure 7 for details). The ellipsoidal neighborhood $\mathcal{E}_\alpha(\lambda_c)$ is the most effective at capturing the greatest variation across the objectives.

Problem	n	q	Neighborhood	MCM	(# Neigh. Points)/ $ \Lambda_m $
ZLT1	3	3	$\mathcal{B}_r(\lambda_c), r = 0.40$	0.0895	0.2392
			$\mathcal{E}_\alpha(\lambda_c), \alpha = 0.10$	0.1529	0.2329
			$\mathcal{E}_\beta(\lambda_c), \beta = 7$	0.0837	0.2251
GRV1	2	3	$\mathcal{B}_r(\lambda_c), r = 0.30$	0.0136	0.1702
			$\mathcal{E}_\alpha(\lambda_c), \alpha = 0.10$	0.1078	0.1639
			$\mathcal{E}_\beta(\lambda_c), \beta = 10$	0.0252	0.1749
VFM1	2	3	$\mathcal{B}_r(\lambda_c), r = 0.23$	0.0260	0.1788
			$\mathcal{E}_\alpha(\lambda_c), \alpha = 0.10$	0.0824	0.1804
			$\mathcal{E}_\beta(\lambda_c), \beta = 13$	0.0546	0.1859
ZLT1 q	5	5	$\mathcal{B}_r(\lambda_c), r = 0.28$	0.0111	0.1026
			$\mathcal{E}_\alpha(\lambda_c), \alpha = 0.10$	0.0974	0.0948
			$\mathcal{E}_\beta(\lambda_c), \beta = 8.5$	0.0176	0.1007

Table 2: Comparison of $\mathcal{B}_r(\lambda_c)$, $\mathcal{E}_\alpha(\lambda_c)$, and $\mathcal{E}_\beta(\lambda_c)$ from the numerical experiments in Subsection 5.4.

6.1 Pareto sensitivity calculation in the constrained case

In this subsection, we extend the *snee* approach developed in Subsection 5.1 to handle constrained MOO problems. Such an extension only requires a recalculation of the sensitivity $\nabla x(\lambda)$ under the presence of constraints. Specifically, instead of deriving $\nabla x(\lambda)$ from the first-order necessary conditions for unconstrained optimality (5.1) in Subsection 5.1, we derive it from the corresponding conditions under the presence of constraints, typically referred to as the first-order KKT conditions, in particular from the equality part of such conditions (the so-called KKT system).

Let us consider the following constrained MOO problem

$$\min_{x \in X} F(x), \quad \text{with } X = \{x \in \mathbb{R}^n \mid c_j(x) \leq 0, j \in I, \text{ and } c_j(x) = 0, j \in E\}, \quad (6.1)$$

where I and E are finite index sets used to denote inequality and equality constraints, respectively. We start with the derivation of $\nabla x(\lambda)$ using the first-order KKT system associated with problem (6.1). Denoting $c_I(x) = (c_j(x), j \in I)$ and $c_E(x) = (c_j(x), j \in E)$, and given $\lambda \in \Lambda$, the Lagrangian function of problem (6.1) is defined as $\mathcal{L}(x, z_I, z_E) = \sum_{i=1}^q \lambda_i f_i(x) + c_I(x)^\top z_I + c_E(x)^\top z_E$, where z_I and z_E are vectors of Lagrange multipliers. In Assumption 6.1 below, we assume that the constraint functions are twice continuously differentiable and there exists a solution $x(\lambda)$ satisfying the KKT conditions for problem (6.1) with associated vectors of multipliers $(z_I(\lambda), z_E(\lambda))$. Specifically, the first-order KKT system for problem (6.1) at $x(\lambda)$ is given by [50, Theorem 3.1.5]

$$\begin{cases} \sum_{i=1}^q \lambda_i \nabla_x f_i(x(\lambda)) + \nabla_x c_I(x(\lambda)) z_I(\lambda) + \nabla_x c_E(x(\lambda)) z_E(\lambda) = 0, \\ z_I(\lambda) \circ c_I(x(\lambda)) = 0, \\ c_E(x(\lambda)) = 0, \end{cases} \quad (6.2)$$

where \circ denotes the element-wise multiplication of two vectors. We do not include the non-negativity of the multipliers in $z_I(\lambda)$ and the satisfaction of the inequality constraints in (6.2) because they are not necessary for the derivation below.

We also assume a well-known set of conditions in constrained optimization theory, as detailed in Assumption 6.1 below, in order to secure the required matrix invertibility in the derivative calculation.

Specifically, we require the linear independence constraint qualification (LICQ), strict complementarity slackness (SCS), and the second-order sufficient condition (SOSC), which are formally stated in Nocedal and Wright [55, Chapter 12, Definitions 12.4-12.5 and Theorem 12.6, respectively] and summarized next. Given Lagrange multipliers $(z_I(\lambda), z_E(\lambda))$ corresponding to a solution $x(\lambda)$ of the KKT conditions, we define the cone of critical directions as:

$$Z(\lambda) = \left\{ d^x \neq 0 : \begin{array}{l} \nabla_x c_i(x(\lambda))^\top d^x \leq 0, \forall i \in I(\lambda) \\ \nabla_x c_i(x(\lambda))^\top d^x = 0, \forall i \in I(\lambda) \text{ with } (z_I(\lambda))_i > 0 \\ \nabla_x c_i(x(\lambda))^\top d^x = 0, \forall i \in E \end{array} \right\}, \quad (6.3)$$

where $I(\lambda)$ denotes the index set of inequality constraints that are active at $x(\lambda)$. LICQ requires that the gradients $\nabla_x c_i(x(\lambda))$, for all $i \in I(\lambda) \cup E$, are linearly independent. SCS requires that for any multipliers $(z_I(\lambda), z_E(\lambda))$ satisfying the KKT conditions at $x(\lambda)$, the strict positivity $(z_I(\lambda))_i > 0$ holds for every $i \in I(\lambda)$. Finally, SOSC requires that for any multipliers $(z_I(\lambda), z_E(\lambda))$ satisfying the KKT conditions at $x(\lambda)$ and for any $d^x \in Z(\lambda)$, with $Z(\lambda)$ as defined in (6.3), the curvature condition $(d^x)^\top \nabla_{xx}^2 \mathcal{L}(x(\lambda), z_I(\lambda), z_E(\lambda)) d^x > 0$ is satisfied.

Assumption 6.1 (Existence of Pareto optimal solutions (LL constrained case))

Let X be defined as in problem (6.1). The constraint functions c_j , with $j \in I \cup E$, are twice continuously differentiable. There exists a solution $x(\lambda)$ satisfying the KKT conditions with associated multipliers $(z_I(\lambda), z_E(\lambda))$ such that the LICQ, SCS, and SOSC are satisfied.

Under Assumption 6.1, based on Fiacco [27, p. 291, Theorem 2.1], the vectors of multipliers $z_I(\lambda)$ and $z_E(\lambda)$ associated with $x(\lambda)$ are unique, and the vector function $w(\lambda) = (x(\lambda), z_I(\lambda), z_E(\lambda))^\top$ is once continuously differentiable for any given λ . Let us now introduce a vector function K such that the KKT system (6.2) can be written as $K(w(\lambda)) = 0$. Applying the chain rule to such an equation, we obtain $\nabla_w K^\top \nabla w^\top = -\nabla_\lambda K^\top$, with

$$\nabla_\lambda K^\top = \begin{pmatrix} \nabla_{x\lambda}^2 \mathcal{L} \\ 0 \\ 0 \end{pmatrix} \text{ and } \nabla_w K^\top = \begin{pmatrix} \nabla_{xx}^2 \mathcal{L} & \nabla_x c_I & \nabla_x c_E \\ z_I \circ \nabla_x c_I^\top & C_I & 0 \\ \nabla_x c_E^\top & 0 & 0 \end{pmatrix}, \quad (6.4)$$

where $\nabla_{x\lambda} \mathcal{L}$ and $\nabla_{xx} \mathcal{L}$ are evaluated at $w(\lambda)$, the Jacobian matrices $\nabla_x c_I^\top$ and $\nabla_x c_E^\top$ are evaluated at $x(\lambda)$, C_I is a diagonal matrix with elements defined by $c_I(x(\lambda))$, and $z_I \circ \nabla_x c_I^\top$ represents a matrix formed by element-wise multiplication of the entries of z_I with the corresponding rows of $\nabla_x c_I^\top$.

Under Assumption 6.1, it is well known that the Jacobian $\nabla_w K^\top$ is non-singular at $w(\lambda)$, see Fiacco [27, p. 294, Eq. (2.4)] or Fiacco and Ishizuka [28, p. 225, Eq. (5.2)]. Therefore, we have

$$\nabla w = (\nabla_x, \nabla_{z_I}, \nabla_{z_E}) = -\nabla_\lambda K \nabla_w K^{-1}. \quad (6.5)$$

Following Giovannelli et al. [35, Subsection 2.2], we can now introduce a matrix $L = (\mathbf{I}_n \quad \mathbf{0})^\top$ to extract the columns of (6.5) that correspond to the $\nabla_x(\lambda)$ term, where \mathbf{I}_n denotes an identity matrix of size n and $\mathbf{0}$ represents a null matrix of dimensions $n \times (|I| + |E|)$, resulting in

$$\nabla x(\lambda) = -\nabla_\lambda K \nabla_w K^{-1} L. \quad (6.6)$$

By applying the chain rule as we did to derive (5.3), but now using the matrix $\nabla x(\lambda)$ from (6.6) instead of (5.2), we obtain that the transpose of the Jacobian matrix of $F(x(\cdot))$ at λ is given by

$$\begin{aligned} \nabla_\lambda (F(x(\lambda))) &= \nabla x(\lambda) \nabla_x F(x(\lambda)) \\ &= -\nabla_\lambda K \nabla_w K^{-1} L (\nabla_x f_1, \dots, \nabla_x f_q). \end{aligned} \quad (6.7)$$

Problem	n	q	Ref.	Objective Functions and Constraints
DAS1	5	2	[19]	$f_1(x_1, \dots, x_5) = x_1^2 + x_2^2 + x_3^2 + x_4^2 + x_5^2$ $f_2(x_1, \dots, x_5) = 3x_1 + 2x_2 - x_3/3 + 0.01(x_4 - x_5)^3$ $c_1(x_1, \dots, x_5) = x_1^2 + x_2^2 + x_3^2 + x_4^2 + x_5^2 - 10 \leq 0$ $c_2(x_1, \dots, x_5) = x_1 + 2x_2 - x_3 - 0.5x_4 + x_5 - 2 = 0$ $c_3(x_1, \dots, x_5) = 4x_1 - 2x_2 + 0.8x_3 + 0.6x_4 + 0.5x_5^2 = 0$
DO2DK	30	2	[9, 20, 24]	$f_1(x) = g_1(x)g_2(x_1) (\sin(\pi x_1/2 + \pi) + 1)$ $f_2(x) = g_1(x)g_2(x_1) (\cos(\pi x_1/2 + \pi) + 1)$ $g_1(x) = 1 + \frac{9}{n-1} \sum_{i=2}^n x_i$ $g_2(x_1) = 5 + 10(x_1 - 0.5)^2 + \cos(2\pi x_1) \cdot 2^{\frac{1}{2}}$ $c_j(x) = -x_j \leq 0, \quad j \in \{1, 2, \dots, n\}$ $c_{n+j}(x) = x_j - r \leq 0, \quad j \in \{1, 2, \dots, n\}$
VFM1constr	2	3		$f_1(x_1, x_2) = x_1^2 + (x_2 - 1)^2$ $f_2(x_1, x_2) = x_1^2 + (x_2 + 1)^2 + 1$ $f_3(x_1, x_2) = (x_1 - 1)^2 + x_2^2 + 2$ $c_1(x_1, x_2) = x_1^2 + x_2^2 - 0.8 \leq 0$ $c_2(x_1, x_2) = (x_1 - 1)^2 + x_2^2 - 1 \leq 0$

Table 3: Constrained test problems (r in DO2DK is an arbitrary positive scalar used to tighten the feasible set).

In (6.7), all gradients $\nabla_x f_i$ are evaluated at $x(\lambda)$, with $i \in \{1, \dots, q\}$, and $\nabla_\lambda K$ and $\nabla_w K$ are evaluated at $w(\lambda)$. Note that matrix $\nabla_\lambda(F(x(\lambda)))$ in (6.7) is no longer symmetric as in the unconstrained case (5.3), but this does not change anything in regards to the applicability of the *snee* approach.

We note that classical multi-objective optimization textbooks often invoke the Kuhn–Tucker constraint qualification (KTCQ), see Ehrgott [26, p. 57, Definition 2.50] and Miettinen [50, p. 38, Definition 3.1.3], originally introduced in Kuhn and Tucker [43]. The KTCQ requires that for every direction in the linearized feasible cone, there exists a smooth feasible arc tangent to that direction, ensuring that the feasible set admits a local differentiable description at the solution. In those references, the KTCQ is used either to establish necessary and sufficient optimality conditions for *properly* efficient solutions, which are points that have bounded trade-offs among the objectives (Ehrgott 2005, p. 51, Definition 2.39), or to guarantee that the KKT system (6.2) holds as a necessary optimality condition when applying the weighted-sum method. We remark that our Assumption 6.1 already subsumes the KTCQ. As shown in Peterson [56, p. 645, Fig. 4], LICQ implies KTCQ, and therefore Assumption 6.1 ensures the validity of the KTCQ invoked in those references.

6.2 MOO constrained test problems

Table 3 specifies the constrained test problems considered in the experiments for Subsection 6.3, along with the number of variables and objectives (i.e., n and q , respectively). Problems DAS1 and DO2DK are well-known in the MOO literature. They have a convex Pareto front, despite some of the objective functions being non-convex.

6.3 Results for knee solutions using Pareto sensitivity in the constrained case

To solve the minimization problem (3.2) in the main step of Algorithm 1, where $\nabla_\lambda(f_i(x(\lambda)))$ and $\nabla_\lambda(f_j(x(\lambda)))$ in the MCF now correspond to the columns of matrix $\nabla_\lambda(F(x(\lambda)))$ in (6.7) instead of (5.3), we again applied the NM and DIRECT algorithms introduced in Section 3, as in Subsection 5.4. Figures 10–12 show the results obtained by the NM algorithm for problems DAS1, DO2DK, and VFM1constr from

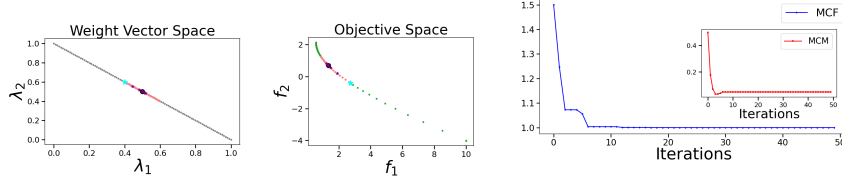


Figure 10: Results for problem DAS1. The left two plots show the weight vector and objective spaces, respectively, when applying the NM algorithm in the main step of Algorithm 1, including the iterates of the optimization process, the neighborhood of weight vectors, and the Pareto sub-front centered at the knee nondominated point. The right plot shows the values of the MCF and MCM over the iterations.

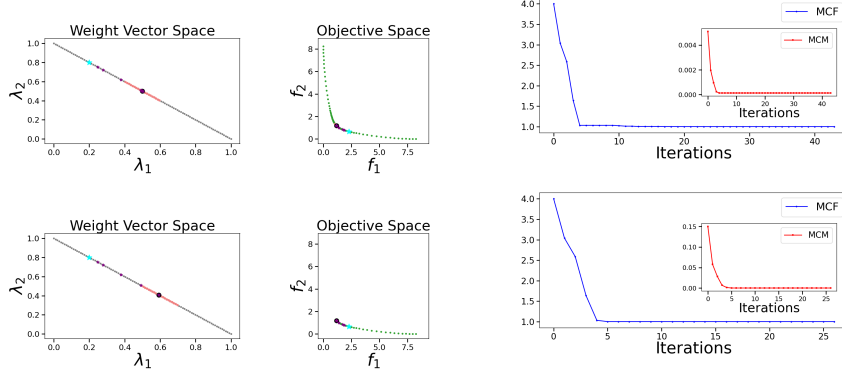


Figure 11: Results for problem DO2DK (upper plots: $r = 1$, lower plots: $r = 0.5$) when applying the NM algorithm in the main step of Algorithm 1 (see the caption of Figure 10 for details).

Table 3. We considered two configurations for problem DO2DK by selecting the constraint right-hand side r from $\{0.5, 1\}$, where 1 corresponds to a larger feasible set and 0.5 results in a tighter feasible set. For the NM algorithm, we arbitrarily used the weight vectors $(0.4, 0.6)$, $(0.2, 0.8)$, and $(0.4, 0.2, 0.4)$ as the initial weight vector λ_0 in Algorithm 1 for problems DAS1, DO2DK, and VFM1 $_{constr}$, respectively. To perform **Step A** and obtain $x(\lambda)$ for a given λ , we solved the weighted-sum problem (2.1) using the SLSQP algorithm [42], which is designed for solving constrained optimization problems through sequential quadratic programming. We ran the SLSQP algorithm implementation available in the Python SciPy library [69], with default parameters.

Similar to Subsection 5.4, the neighborhoods of weight vectors shown in the figures are the ellipsoidal ones, centered at the best iterate returned by the algorithm. For all the problems, using a fixed neighborhood size α results in ellipsoidal neighborhoods that either have no elements or contain the entire simplex set at certain iterations. Therefore, we adopt the same adaptive rule used for GRV2 in Subsection 5.3. Again, the neighborhoods are required only for computing the MCM and not for the MCF.

Figure 10 and the upper plots of Figure 11 show that the knee nondominated points for problem DAS1 and for problem DO2DK when $r = 1$ (i.e., the feasible set is relatively large) lie in the intermediate region of the Pareto front. In contrast, in the lower plots of Figure 11 and in Figure 12, our *snee* approach leads to knee nondominated points that correspond to points on the boundary of the Pareto front. Similar to Subsection 5.3, the reason why we do not observe a knee nondominated point in the intermediate region for DO2DK with $r = 0.5$ and VFM1 $_{constr}$ is due to the lack of a bulge in the Pareto front within the interior of the feasible set. Instead, the normal boundary intersection method would have returned a point in the intermediate region, regardless of the presence of a bulge.

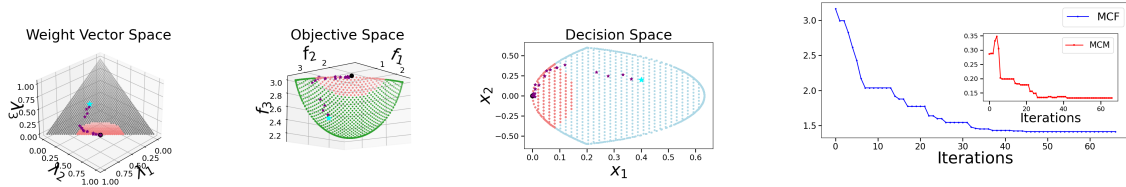


Figure 12: Results for problem $VFM1constr$ when applying the NM algorithm in the main step of Algorithm 1. The figure includes plots of the weight vector, objective, and decision spaces, including the iterates of the optimization process, the neighborhood of weight vectors, the Pareto sub-front centered at the knee nondominated point, and the neighborhood of Pareto optimal solutions centered at the knee solution, as well as the values of the MCF and MCM over the iterations.

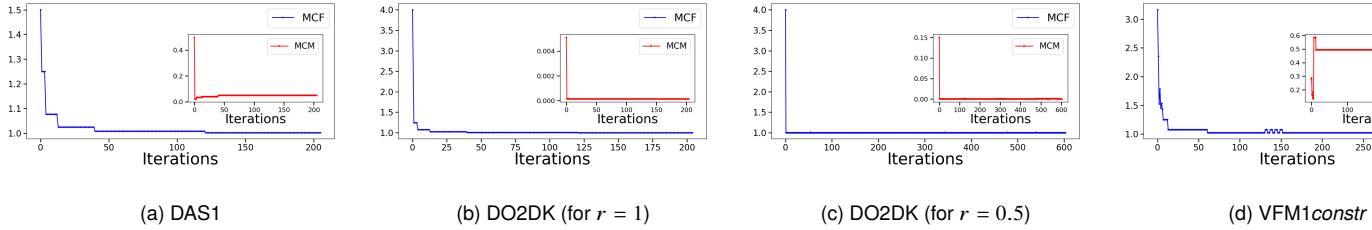


Figure 13: Plots that show the values of the MCF and MCM over the iterations when applying the DIRECT algorithm in the main step of Algorithm 1.

For the DIRECT algorithm, we include in Figure 13 the plots showing the values of the MCF and MCM over the iterations for all constrained problems from Table 3, and we do not represent the weight vector, objective, and decision spaces because the final solution to the minimization problem (3.2) in the main step of Algorithm 1 is nearly identical to that of the NM algorithm, except for problem $VFM1constr$. For $VFM1constr$, the nondominated point found by DIRECT lies on the west boundary of the Pareto front (see objective space of Figure 14), whereas the nondominated point found by NM lies on the upper boundary, as shown in the objective space of Figure 12. Such differences arise because the MCF is non-convex, causing the NM algorithm to get stuck in local minimizers, while the DIRECT algorithm finds global minimizers (or, at least, better local minimizers than NM). It becomes then evident that knee solutions can have a local or global nature. Interestingly, the results for problem $VFM1constr$ shown in plot d) of Figure 13 suggest that a minimizer of the MCF may not correspond to a minimizer of the MCM. This discrepancy arises because the ellipsoidal neighborhood becomes degenerate at the weight vector corresponding to the optimal solution of problem (3.2) (and nearby points), as shown in the objective space of Figure 14. The degeneracy occurs because the matrix $\nabla_{\lambda}(F(x(\lambda)))$ is highly ill-conditioned, with two of its three eigenvalues close to zero, resulting in an elongated ellipsoid that inflates the value

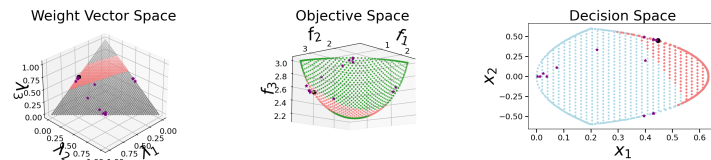


Figure 14: Results for problem $VFM1constr$ when applying the DIRECT algorithm in the main step of Algorithm 1. The plots show the weight vector, objective, and decision spaces, including the iterates of the optimization process, the neighborhood of weight vectors, the Pareto sub-front centered at the knee nondominated point, and the neighborhood of Pareto optimal solutions centered at the knee solution.

of the MCM. This observation confirms that minimizing the MCM instead of the MCF is not a reliable approach for finding knee solutions, as previously noted in Remark 5.1 of Subsection 5.3.

7 Concluding remarks and future work

In this paper, we showed how to use first-order rates of variation of Pareto optimal solutions to better understand the tradeoffs of a Pareto front in multi-objective optimization. We have used such sensitivity rates to provide an answer to the open question of how to rigorously compute knee solutions, i.e., solutions corresponding to nondominated points where a small improvement in any objective leads to a large deterioration in at least one other objective. Based on the observation that nondominated points corresponding to such solutions lie where slopes in a Pareto front are leveled, we introduced formulation (3.2) to accurately identify the desired knee solution. The corner stone of our approach is the ability to compute the gradient $\nabla_{\lambda}(f_i(x(\lambda)))$ of each individual function $f_i(x(\cdot))$ through the rate of variation $\nabla x(\lambda)$ of the Pareto optimal solution $x(\lambda)$, where λ denotes a vector of objective weights. The formulation (3.2) was used to compute knee solutions following their verbal definition regardless of the presence of constraints. We called our approach *snee* to emphasize the use of Pareto sensitivity in the calculation of the derivatives of $F(x(\lambda))$.

We also showed in this paper how to compute the most-changing Pareto sub-fronts around a nondominated point. Such sub-fronts are obtained from neighborhoods of weight vectors constructed using the pseudo-inverse of the Jacobian matrix of the vector function $F(x(\cdot))$ and include nondominated points that are distributed along directions of maximum change. We considered the neighborhood achieving the highest value of the MCM to be the most effective, and we evaluated the proposed neighborhoods numerically rather than analytically, as such a theoretical study would be out of the scope of this paper.

The techniques used in our approach are still restricted to scalarized methods. In the current paper, we explored the weighted-sum method, which requires convexity of the objective functions in F for a complete coverage of the Pareto front. Our approach can be extended to the ε -constrained method, which converts a multi-objective problem into a single-objective constrained problem where one objective is optimized subject to constraints requiring the other objectives to be below varying thresholds. Given a positive threshold ε and denoting the corresponding Pareto optimal solution as $x(\varepsilon)$, one can consider a neighborhood of ε to determine a Pareto neighborhood around $x(\varepsilon)$. To compute knee solutions using our *snee* approach, one can consider a reformulation of problem (3.2) in terms of ε . Although the ε -constrained method does not explicitly require convexity for a complete coverage of the Pareto front, it requires a global solution of a constrained optimization problem. Therefore, our future work will focus on exploring techniques that do not rely on scalarized methods.

Acknowledgments

This work is partially supported by the U.S. Air Force Office of Scientific Research (AFOSR) award FA9550-23-1-0217 and the U.S. Office of Naval Research (ONR) award N000142412656.

References

- [1] B. Afsar, K. Miettinen, and F. Ruiz. Assessing the performance of interactive multiobjective optimization methods: A survey. *ACM Computing Surveys*, 54:85:1–85:27, 2021.

- [2] K. A. Andersen, T. K. Boomsma, B. Efkes, and N. Forget. Sensitivity analysis of the cost coefficients in multiobjective integer linear optimization. *Management Science*, 71:1120–1137, 2024.
- [3] C. Audet and W. Hare. *Derivative-Free and Blackbox Optimization*. Springer Series in Operations Research and Financial Engineering. Springer, Cham, 2017. With a foreword by John E. Dennis Jr.
- [4] C. Audet, J. Bignon, D. Cartier, S. Le Digabel, and L. Salomon. Performance indicators in multiobjective optimization. *European Journal of Operational Research*, 292:397–422, 2021.
- [5] S. Bechikh, L. Ben Said, and K. Ghédira. Searching for knee regions in multi-objective optimization using mobile reference points. In *Proceedings of the 2010 ACM Symposium on Applied Computing, SAC '10*, page 1118–1125, New York, NY, USA, 2010. Association for Computing Machinery.
- [6] N. Boehmer and M. T. Wittmann. Picking a representative set of solutions in multiobjective optimization: Axioms, algorithms, and experiments. *arXiv e-prints*, art. arXiv:2511.10716, November 2025.
- [7] M. Boresta, T. Giovannelli, and M. Roma. Managing low-acuity patients in an emergency department through simulation-based multiobjective optimization using a neural network metamodel. *Health Care Management Science*, 27:415–435, 2024.
- [8] L. Bottou, F. E. Curtis, and J. Nocedal. Optimization methods for large-scale machine learning. *SIAM Rev.*, 60:223–311, 2018.
- [9] J. Branke, K. Deb, H. Dierolf, and M. Osswald. Finding knees in multi-objective optimization. In *Parallel Problem Solving from Nature - PPSN VIII*, pages 722–731, Berlin, Heidelberg, 2004. Springer Berlin Heidelberg.
- [10] W.J. Burke, H.M. Merrill, F.C. Schweppe, B.E. Lovell, M.F. McCoy, and S.A. Monohon. Trade off methods in system planning. *IEEE Transactions on Power Systems*, 3:1284–1290, 1988. doi: 10.1109/59.14593.
- [11] L. Chen, H. Fernando, Y. Ying, and T. Chen. Three-Way Trade-Off in Multi-Objective Learning: Optimization, Generalization and Conflict-Avoidance. *arXiv e-prints*, art. arXiv:2305.20057, May 2023.
- [12] T. Chen, Y. Sun, and W. Yin. A Single-Timescale Stochastic Bilevel Optimization Method. *arXiv e-prints*, art. arXiv:2102.04671, February 2021.
- [13] Y. Chen and A. Zhou. Multiobjective portfolio optimization via pareto front evolution. *Complex & Intelligent Systems*, 8:4301–4317, 2022.
- [14] G. Chiandussi, M. Codegone, S. Ferrero, and F.E. Varesio. Comparison of multi-objective optimization methodologies for engineering applications. *Computers & Mathematics with Applications*, 63:912–942, 2012.
- [15] K. L. Chung. On a stochastic approximation method. *Annals of Mathematical Statistics*, 25:463 – 483, 1954.
- [16] A. R. Conn, K. Scheinberg, and L. N. Vicente. *Introduction to Derivative-Free Optimization*. MPS/SIAM Book Series on Optimization, SIAM, Philadelphia, USA, 2009.

- [17] A. L. Custódio, K. Scheinberg, and L. N. Vicente. Chapter 37: Methodologies and software for derivative-free optimization. In *Advances and Trends in Optimization with Engineering Applications*, pages 495–506. SIAM, 2017.
- [18] I. Das. On characterizing the “knee” of the pareto curve based on normal-boundary intersection. *Structural Optimization*, 18:107–115, 1999.
- [19] I. Das and J. E. Dennis. Normal-boundary intersection: A new method for generating the Pareto surface in nonlinear multicriteria optimization problems. *SIAM Journal on Optimization*, 8:631–657, 1998.
- [20] K. Deb. Multi-objective genetic algorithms: Problem difficulties and construction of test problems. *Evolutionary Computation*, 7:205–230, 1999.
- [21] K. Deb. *Multi-objective evolutionary algorithms: Introducing bias among Pareto-optimal solutions*, page 263–292. Springer-Verlag, Berlin, Heidelberg, 2003.
- [22] K. Deb and S. Gupta. Understanding knee points in bicriteria problems and their implications as preferred solution principles. *Engineering Optimization*, 43, 08 2010.
- [23] K. Deb, A. Pratap, S. Agarwal, and T. Meyarivan. A fast and elitist multiobjective genetic algorithm: NSGA-II. *IEEE Transactions on Evolutionary Computation*, 6:182–197, 2002.
- [24] K. Deb, L. Thiele, M. Laumanns, and E. Zitzler. Scalable multi-objective optimization test problems. In *Proceedings of the 2002 Congress on Evolutionary Computation. CEC’02 (Cat. No.02TH8600)*, volume 1, pages 825–830 vol.1, 2002.
- [25] E. Demir, T. Bektaş, and G. Laporte. The bi-objective pollution-routing problem. *European Journal of Operational Research*, 232:464–478, 2014.
- [26] M. Ehrgott. *Multicriteria Optimization*, volume 491. Springer Science & Business Media, Berlin, 2005.
- [27] A. V. Fiacco. Sensitivity analysis for nonlinear programming using penalty methods. *Mathematical Programming*, 10:287–311, 1976.
- [28] A. V. Fiacco and Y. Ishizuka. Sensitivity and stability analysis for nonlinear programming. *Annals of Operations Research*, 27:215–235, 1990.
- [29] P. J. Fleming, R. C. Purshouse, and R. J. Lygoe. Many-objective optimization: An engineering design perspective. In *Evolutionary Multi-Criterion Optimization*, pages 14–32, Berlin, Heidelberg, 2005. Springer Berlin Heidelberg.
- [30] R. Fletcher. *Practical Methods of Optimization*. Wiley, Chichester; New York, 1987.
- [31] S. Ghadimi and M. Wang. Approximation methods for bilevel programming. *arXiv e-prints*, art. arXiv:1802.02246, 2018.
- [32] T. Giovannelli and L. N. Vicente. An integrated assignment, routing, and speed model for roadway mobility and transportation with environmental, efficiency, and service goals. *Transportation research part C: Emerging technologies*, 152:104144, 2023.

- [33] T. Giovannelli, G. D. Kent, and L. N. Vicente. Bilevel optimization with a multi-objective lower-level problem: Risk-neutral and risk-averse formulations. *Optimization Methods and Software*, pages 1–23, 2024.
- [34] T. Giovannelli, G. D. Kent, and L. N. Vicente. A stochastic gradient method for trilevel optimization. *arXiv e-prints*, art. arXiv:2505.06805, May 2025.
- [35] T. Giovannelli, G. D. Kent, and L. N. Vicente. Inexact bilevel stochastic gradient methods for constrained and unconstrained lower-level problems. *Journal of Global Optimization*, 92:569–614, 2025.
- [36] T. Giovannelli, Griffin D. Kent, and L. N. Vicente. Inexact bilevel stochastic gradient methods for constrained and unconstrained lower-level problems. *Journal of Global Optimization*, 92:569–614, 2025.
- [37] J. Hakanen and R. Allmendinger. Multiobjective optimization and decision making in engineering sciences. *Optimization and Engineering*, 22:1031–1037, 2021.
- [38] S. Huband, P. Hingston, L. Barone, and R. Lyndon While. A review of multiobjective test problems and a scalable test problem toolkit. *IEEE Transactions on Evolutionary Computation*, 10:477–506, 2006.
- [39] M. Jameel, H. Merah, A. M. A. El-latif, and et al. Multiobjective starfish optimization algorithm for engineering design and optimal power flow problems. *Scientific Reports*, 16:3302, 2026.
- [40] K. Ji, J. Yang, and Y. Liang. Bilevel Optimization: Convergence Analysis and Enhanced Design. *arXiv e-prints*, art. arXiv:2010.07962, October 2020.
- [41] D. R. Jones, C. D. Perttunen, and B. E. Stuckman. Lipschitzian optimization without the lipschitz constant. *Journal of Optimization Theory and Applications*, 79:157–181, 1993.
- [42] D. Kraft. A software package for sequential quadratic programming. Technical Report DFVLR-FB 88-28, DLR German Aerospace Center — Institute for Flight Mechanics, Köln, Germany, 1988.
- [43] H. W. Kuhn and A. W. Tucker. Nonlinear programming. In Jerzy Neyman, editor, *Proceedings of the Second Berkeley Symposium on Mathematical Statistics and Probability*, pages 481–492. University of California Press, Berkeley, California, 1951.
- [44] J. Larson, M. Menickelly, and S. M. Wild. Derivative-free optimization methods. *Acta Numerica*, 28:287–404, 2019.
- [45] J. D. Lawrence. *A Catalog of Special Plane Curves*. Dover Publications, New York, 1972. ISBN 9780486602887. Reprint of the original edition; includes a comprehensive treatment of classical plane curves such as Cassini ovals.
- [46] X. Lin, H.-L. Zhen, Z. Li, Q.-F. Zhang, and S. Kwong. Pareto multi-task learning. In *Advances in Neural Information Processing Systems*, volume 32. Curran Associates, Inc., 2019.
- [47] X. Lin, Y. Liu, X. Zhang, F. Liu, Z. Wang, and Q. Zhang. Few for many: Tchebycheff set scalarization for many-objective optimization. *arXiv e-prints*, art. arXiv:2405.19650, May 2024.

- [48] S. Liu and L. N. Vicente. The Sharpe predictor for fairness in machine learning. *arXiv e-prints*, art. arXiv:2108.06415, August 2021.
- [49] S. Liu and L. N. Vicente. Accuracy and fairness trade-offs in machine learning: A stochastic multi-objective approach. *Computational Management Science*, 19:513–537, 2022.
- [50] K. Miettinen. *Nonlinear Multiobjective Optimization*, volume 12 of *International Series in Operations Research & Management Science*. Kluwer Academic Publishers, Boston, USA, 1999.
- [51] A. Navon, A. Shamsian, G. Chechik, and E. Fetaya. Learning the Pareto Front with Hypernetworks. *arXiv e-prints*, art. arXiv:2010.04104, October 2020.
- [52] J. A. Nelder and R. Mead. A simplex method for function minimization. *Computer Journal*, 7: 308–313, 1965.
- [53] Y. Nesterov. *Lectures on Convex Optimization*. Springer Publishing Company, Incorporated, 2nd edition, 2018. ISBN 3319915770.
- [54] Y. Nesterov and V. Spokoiny. Random gradient-free minimization of convex functions. *Foundations of Computational Mathematics*, 17:527–566, 2017.
- [55] J. Nocedal and S. J. Wright. *Numerical Optimization*. Springer-Verlag, Berlin, second edition, 2006.
- [56] D. W. Peterson. A review of constraint qualifications in finite-dimensional spaces. *SIAM Review*, 15:639–654, 1973.
- [57] D. Ríos Insua. *Sensitivity Analysis in Multi-objective Decision Making*, volume 347 of *Lecture Notes in Economics and Mathematical Systems*. Springer, Berlin, Heidelberg, 1990.
- [58] H. Robbins and S. Monro. A stochastic approximation method. *Ann. Math. Statist.*, 22:400–407, 1951.
- [59] W. Rudin. *Principles of mathematical analysis*. McGraw-Hill Book Company, Inc., New York-Toronto-London, 1953.
- [60] J. Sacks. Asymptotic distribution of stochastic approximation procedures. *Annals of Mathematical Statistics*, 29:373 – 405, 1958.
- [61] W. F. Sharpe. Mutual fund performance. *The Journal of Business*, 39:119–138, 1966.
- [62] P. K. Shukla, M. A. Braun, and H. Schmeck. Theory and algorithms for finding knees. In *Evolutionary Multi-Criterion Optimization*, pages 156–170, Berlin, Heidelberg, 2013. Springer Berlin Heidelberg.
- [63] A. Sinha and K. Deb. Towards understanding evolutionary bilevel multi-objective optimization algorithm. *IFAC Proceedings Volumes*, 42:338–343, 2009.
- [64] M. C. Steinbach. Markowitz revisited: Mean-variance models in financial portfolio analysis. *SIAM Review*, 43:31–85, 2001.
- [65] R. H. Stewart, T. S. Palmer, and B. DuPont. A survey of multi-objective optimization methods and their applications for nuclear scientists and engineers. *Progress in Nuclear Energy*, 138:103830, 2021. ISSN 0149-1970.

- [66] A. Sulas, D. Maringer, and S. Paterlini. Systemic risk from overlapping portfolios: A multi-objective optimization framework. *International Review of Financial Analysis*, 97:103794, 2025.
- [67] T. Tanino. Sensitivity analysis in multiobjective optimization. *J. Optim. Theory Appl.*, 56:479–499, mar 1988.
- [68] E. Triantaphyllou. *Multi-criteria Decision Making Methods: A Comparative Study*, volume 44 of *Applied Optimization*. Springer New York, NY, 1 edition, 2000. Springer Science+Business Media Dordrecht 2000.
- [69] P. Virtanen, R. Gommers, T. E. Oliphant, M. Haberland, T. Reddy, D. Cournapeau, E. Burovski, P. Peterson, W. Weckesser, J. Bright, and et al. SciPy 1.0: Fundamental Algorithms for Scientific Computing in Python. *Nature Methods*, 17:261–272, 2020.
- [70] H. Wang, Olhofer M., and Y. Jin. A mini-review on preference modeling and articulation in multi-objective optimization: current status and challenges. *Complex & Intelligent Systems*, 3:233–245, 2017.
- [71] L. Weerasena, M. M. Wiecek, and B. Soylu. An algorithm for approximating the pareto set of the multiobjective set covering problem. *Annals of Operations Research*, 248:493–514, 2017.
- [72] J. Wu and S. Azarm. Metrics for quality assessment of a multiobjective design optimization solution set. *Journal of Mechanical Design*, 123:18–25, 01 2000.
- [73] W. Zhang, K. Cao, S. Liu, and B. Huang. A multi-objective optimization approach for health-care facility location-allocation problems in highly developed cities such as hong kong. *Computers, Environment and Urban Systems*, 59:220–230, 2016.
- [74] X. Zhang, Y. Tian, and Y. Jin. A knee point-driven evolutionary algorithm for many-objective optimization. *IEEE Transactions on Evolutionary Computation*, 19:761–776, 2015.